Title

CO2 plume evolution in a depleted natural gas reservoir: Modeling of conformance uncertainty reduction over time

Authors

Doughty, Christine

Oldenburg, Curtis M

Publication Date

2020-06-01

DOI

10.1016/j.ijggc.2020.103026

CO_2 Plume Evolution in a Depleted Natural Gas Reservoir:

Modeling of Conformance Uncertainty Reduction Over Time

Christine Doughty and Curtis M. Oldenburg

Earth and Environmental Sciences, Lawrence Berkeley National Laboratory

Berkeley, CA 94720 USA

February 12, 2020

Keywords: Geologic carbon sequestration; post-injection site care; uncertainty; conformance; Class VI; depleted gas reservoir, TOUGH3

Abstract

Uncertainty in the long-term fate of CO_2 injected for geologic carbon sequestration (GCS) is a significant barrier to the adoption of GCS as a greenhouse-gas emission-mitigation for industry and regulatory agencies alike. We present a modeling study that demonstrates that the uncertainty in forecasts of GCS site performance decreases over time as monitoring data are used to update operational models. We consider a case study of GCS in a depleted natural gas reservoir, with CO_2 injection occurring over 20 years, with a 50-year post-injection site care period. We constructed a detailed model to generate the *actual* model output, which is considered synthetic observation data. A series of simpler *operational* models based on limited data and assumptions about how an operator would model such a site are then run and compared against actual model output at specific monitoring points after one year, two years, etc. The operational model is updated and improved using the synthetic observation data from the actual model at the same time intervals. Model parameter values and model features needed to be updated over time to improve matches to the actual model. These kinds of model adjustments would be a normal part of reservoir engineering and site management at GCS sites. Uncertainty in two key measures related to site performance decreases with time: extent of the CO_2 plume up-dip migration, and radial extent of the pressure pulse. This conclusion should help allay the concerns of industry and regulators about uncertainty in long-term fate of CO_2 at GCS sites.

1. Introduction

In order to make a substantial impact in reducing greenhouse gas emissions, geologic carbon sequestration (GCS) will need to involve injection of millions of tonnes of CO_2 at many sites worldwide over several decades. Following injection there will be a post-injection site care (PISC) period during which monitoring will be carried out so that the operator can ensure that

40 CO_2 storage is permanent and that the project is not impacting underground sources of drinking
41 water (USDW). The U.S. EPA in its Class VI CO_2 injection well permitting regulation specifies
42 50 years as a period over which monitoring should be carried out during PISC (U.S. EPA, 2008),
43 while the California Air Resources Board (2017) is suggesting a period of 100 years is needed
44 for monitoring to ensure permanence. Given the lack of experience with industrial-scale CO_2
45 injection for GCS, the costs of multi-decadal monitoring operations during PISC are difficult to
46 forecast, and this uncertainty is increasing the estimated lifecycle cost of GCS. Given the
47 widespread agreement that GCS must be part of the solution for reducing effective greenhouse
48 gas emissions (IPCC, 2018), there is strong motivation to understand more about the long-term
49 evolution of injected CO_2 in the subsurface and the evolution of uncertainty in CO_2 storage as
50 large-scale projects mature over time.

51 To address the above lack of knowledge, we have undertaken a modeling and simulation study
52 that makes use of a synthetic GCS project about which everything is known by virtue of detailed
53 numerical simulations, which we denote the *actual* model. However, we assume that our
54 knowledge of the GCS project is limited to actual model results that represent observations made
55 at a limited number of monitoring wells, for a limited period of time. This limited information is
56 used to develop a series of *operational* models of the GCS project, whose long-term predictions
57 for CO_2 plume evolution are then compared with those of the detailed model representing the
58 actual system. In this study, this procedure is repeated periodically, with more synthetic data
59 becoming available as time progresses. The idea is that by examining synthetic monitoring data
60 from the virtual GCS project at a series of times, we can determine how operational models
61 improve over time as more data become available, and thereby reduce forecast uncertainty over
62 time. With this understanding of uncertainty evolution in hand, we can assess how much

63 uncertainty there is in typical model-based forecasts of CO_2 plume and pressure evolution and
64 how uncertainty evolves over time for the given injection scenario.

65 The example studied here considers a depleted natural gas reservoir system typical of large GCS
66 opportunities in the Sacramento River Delta region of California. It was previously suggested
67 that depleted gas reservoirs are, by virtue of their proven capacity to store a buoyant gas (i.e.,
68 methane), low-hanging fruit for large-scale GCS (Oldenburg et al., 2001). The objective of this
69 study is to demonstrate the reduction in uncertainty over time of forecasts of plume properties as
70 the updated operational models incorporate more synthetic observation data (the actual model
71 output) and become more detailed and skilled at forecasting over time. The overall impact of
72 these findings may have bearing on the time periods required for PISC. In addition, our study
73 informs the needed monitoring intensity which also may be confidently estimated to decline with
74 time based on our study. Finally, results of the study may cause risk-averse stakeholders to gain
75 tolerance for uncertainty in early forecasts of a GCS project, knowing uncertainty will diminish
76 over time.

77 **2. Background**

78 A survey of the literature on uncertainty reduction in GCS and other hydrologic systems
79 uncovers a large body of research based on sophisticated approaches such as modified Kalman
80 filters (Chen and Zhang, 2006; Sun et al., 2009), enhanced Monte Carlo methods (Keating et al.,
81 2010), and polynomial chaos expansion (Oladyshkin et al., 2011; Walter et al., 2012). Our study
82 does not utilize any sophisticated, elegant, or new techniques. The novelty is instead in the use of
83 a large synthetic system as a proxy for a real system, and the application to GCS where there is
84 an urgent need for understanding of long-term evolution of model forecast uncertainty.

Our study is also novel in that we couch uncertainty reduction in forecasts of CO_2 storage risk in terms of reduction in uncertainty of conformance. The concept of conformance combines concordance and performance (e.g., Chadwick and Noy, 2015; Oldenburg, 2018). In the GCS context, concordance is the degree to which model forecasts of plume extent, pressure rise, etc. match observations, and performance is the degree to which the storage system is performing as designed. For example, models should be able to history-match observations (known in some fields as hindcasting), and the monitoring system should be indicating that CO_2 is filling the intended storage reservoir, not leaking, not impacting underground sources of drinking water (USDW), and not causing pressure rise above tolerable ranges. If all of these conditions are met, we can say the system is conforming. In terms of regulators and stakeholders, a conforming GCS project is a successful GCS project. Nevertheless, as with all subsurface technologies, there is uncertainty involved in the assessment of conformance, and this uncertainty must be understood in order to understand the robustness of conformance assessment (e.g., Harp et al., 2019).

Further to the above, we address in this study the reduction in uncertainty in forecasts of conformance. Conformance forecasts are uncertain because the underlying model predictions are uncertain. In the present study, we use synthetic system performance data to quantify the uncertainty in operational model forecasts and make conclusions about how that uncertainty diminishes over time as the operational model is improved as more synthetic observation data become available over time. Therefore, this study addresses the question of the reduction in uncertainty (during GCS operations as models are improved) of forecasts of conformance. Additional uncertainty enters into conformance assessments from the incomplete knowledge arising from imprecise monitoring observations. We have not included this aspect into the study

in order to focus attention on the uncertainty that diminishes as experience with a system is gained over time and as that experience is incorporated into operational models.

3. Approach

The approach we take involves use of a detailed model of a GCS scenario at a specific site, which we denote the *actual* model, to generate a set of synthetic data that represent observations from several monitoring wells. We assume that the operators of the project would have an *operational* model of the CO_2 injection and storage system that they use for injection design, risk assessment, monitoring design, and permitting. Assuming the project is permitted and injection begins, observations and performance data would be used to update the operational model. This study carries out this observation-model update loop to demonstrate the reduction in uncertainty of operational model forecasts over time, by comparing them to synthetic data generated with the actual model. The procedure is outlined in flow chart form in Figure 1 where the CO_2 injection period is 20 years and the PISC period is assumed to be 50 years following the U.S. EPA Class VI regulation (U.S. EPA, 2008).

We first define an injection scenario and design a logical and practical monitoring program. We then create a detailed numerical model (denoted the actual model) and simulate 20 years of large-scale CO_2 injection and 180 years of shut-in to create synthetic performance and monitoring data. This synthetic data set is then set aside. Using a subset of characterization data, we then create a simplified operational model conceived as being similar to one that an operator would develop based on available data, which are assumed to be much more limited than the data that went into defining the actual model. As shown in the flowchart of Figure 1, we use the operational model to simulate injection and monitoring for the first year. Based on a comparison

of operational model monitoring observations to actual model monitoring observations (assumed to be 100% correct, i.e., no measurement uncertainty) at discrete monitoring well locations at the end of Year 1, we then adjust the simplified operational model (history match) and make a forecast for Year 2. We then repeat this process over the years of injection (see Figure 1). We demonstrate by this approach that the simplified operational model becomes better and better over time (uncertainty decreases) in making long-term forecasts, as observations are incorporated into the model to improve its annual forecasting skill.

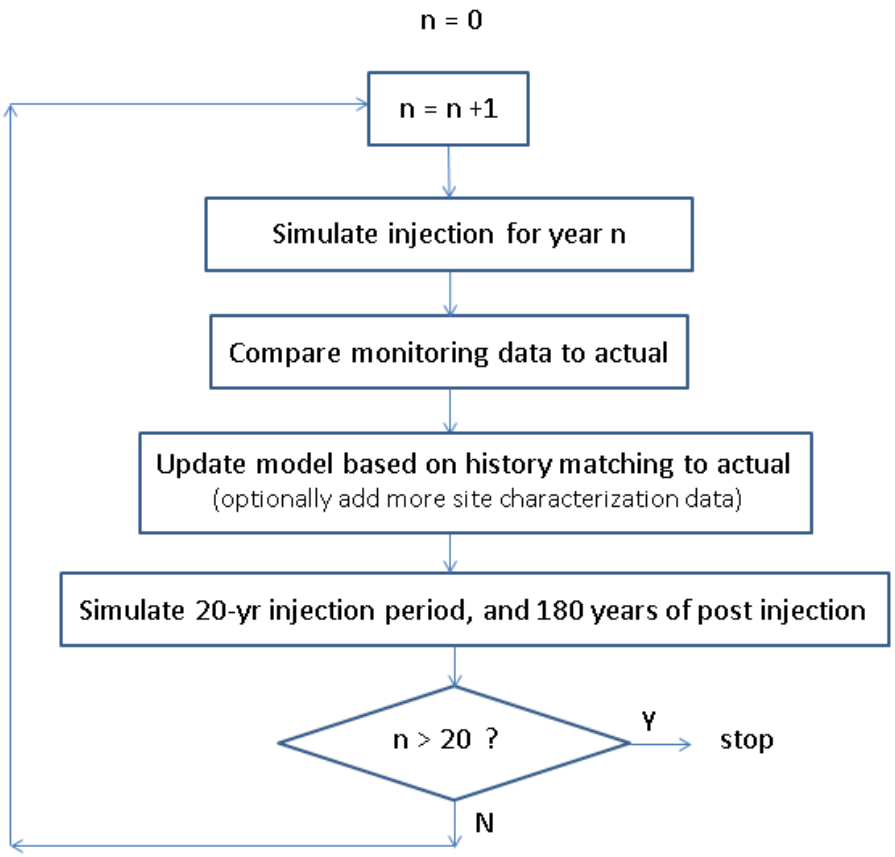

Figure 1. Flow chart showing the updating and forward simulation steps for the operational model used in the study.

3.1 Actual Depleted Gas Reservoir System

California Delta Geologic Setting

The simulated system we use as the actual model has properties based on a site that is representative of typical large-scale depleted natural gas (CH_4) reservoirs in the Sacramento River Delta area of California. This region in the southwestern Sacramento Valley is within 50 miles (80 km) of several San Francisco Bay Area refineries that may someday capture CO_2 for GCS. An unpublished regional-scale geologic model (see Burton et al., 2016) provides the overall geologic structure. The sandstone storage reservoir we consider has variable thickness averaging approximately 500 m at depths of 1000-2000 m. The storage reservoir is composed of high-permeability sandstone with local low-permeability zones; it is generally dipping at 1.6º to the SW, and is capped by an impermeable shale over an undulating reservoir top surface. Layering within the sandstone storage reservoir is based on a well log (see supplemental material, Figure S1) from a Sacramento River Delta well (Burton et al., 2016). Porosity ranges from 0.25 to 0.35, horizontal permeability ranges from 5 to 500 mD, and vertical permeability ranges from 0.02 to 100 mD. We add stochastic heterogeneity to each model layer using GSLIB (Deutsch and Journel, 1992) (Figure 2 and supplemental material, Figure S2). Two sub-vertical faults are included that inhibit cross-flow, but enhance flow parallel to the faults. The depth of the top of the storage formation is shown in Figure 3, revealing the dip and attic regions in the storage reservoir. The water in the system initially is assumed to contain dissolved CH_4, consistent with it being a depleted gas reservoir. While many of the larger natural gas reservoirs in the Sacramento River Delta area are depleted, free-phase CH_4 is often still present in localized attic regions trapped up against the caprock (Figure 4) and we assume that is the case here (see supplemental material for a complete description of the initial conditions used for the actual model). As will be shown by the modeling results below, injected CO_2 buoyantly pinned in the

upper-most regions of the storage reservoir tends to migrate updip, generally in a northeasterly direction(Figure 3) toward the shallowest regions of the reservoir and into attics in the reservoir that originally contain residual free-phase CH_4.

Simulations were carried out using the numerical simulator TOUGH3 (Jung et al., 2017) with equation of state module EOS7C; (Oldenburg et al., 2004). A summary of TOUGH3/EOS7C capabilities is given in the supplemental material, along with a description and illustration of the numerical grid (Figure S3), and comments on processes not included in the actual model.

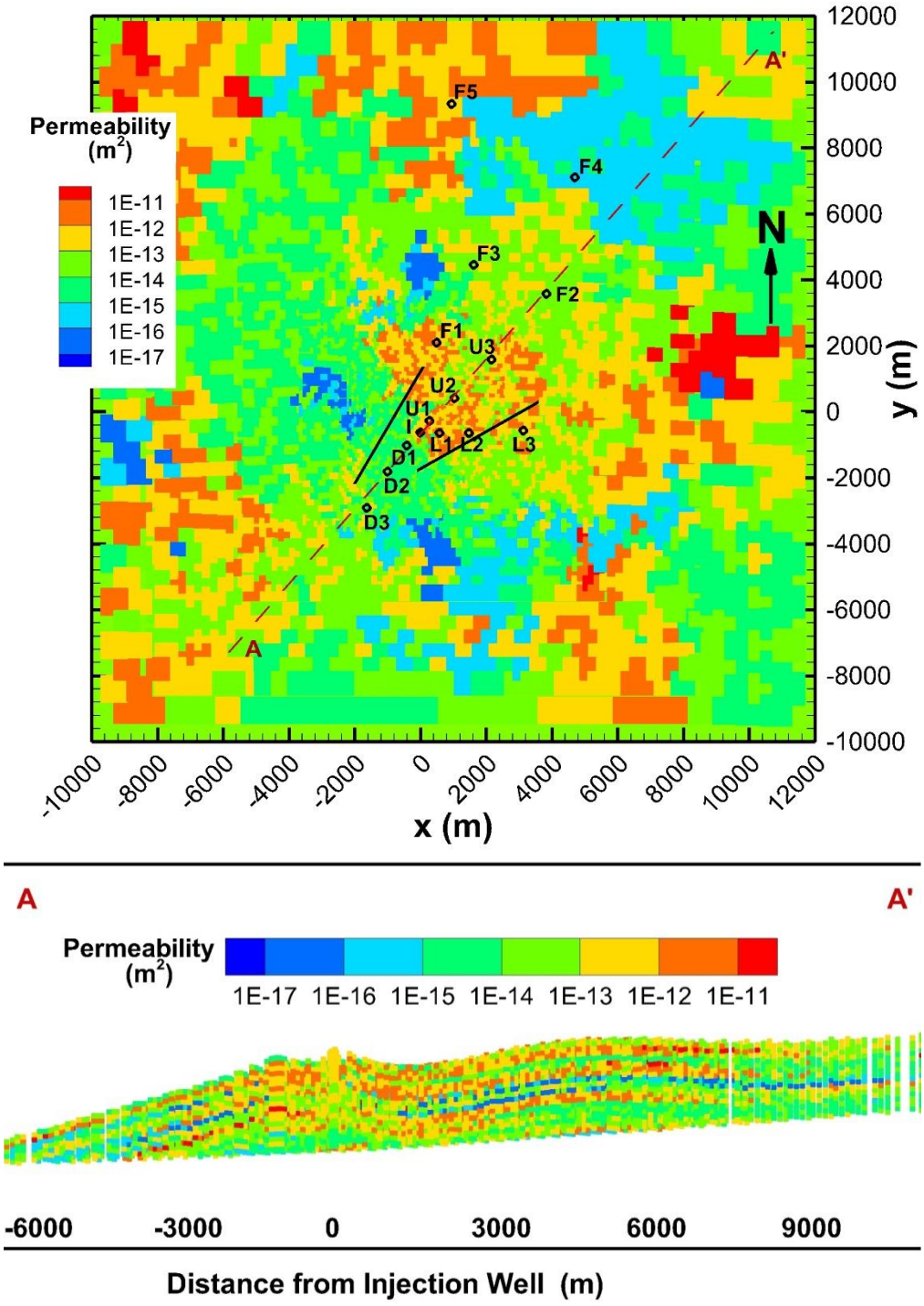

171

172

173 *Figure 2. (top) The center region of the top layer of the storage reservoir in the actual model,*
174 *illustrating the heterogeneous permeability distribution along with monitoring wells (open black*
175 *circles) and the injection well (closed black circle). Two vertical faults are shown as black line*
176 *segments. (bottom) Vertical cross-section at the location of the dashed line shown in the top*
177 *frame showing the reservoir heterogeneity and locally closed structures (attics). Vertical*
178 *exaggeration is two times.*

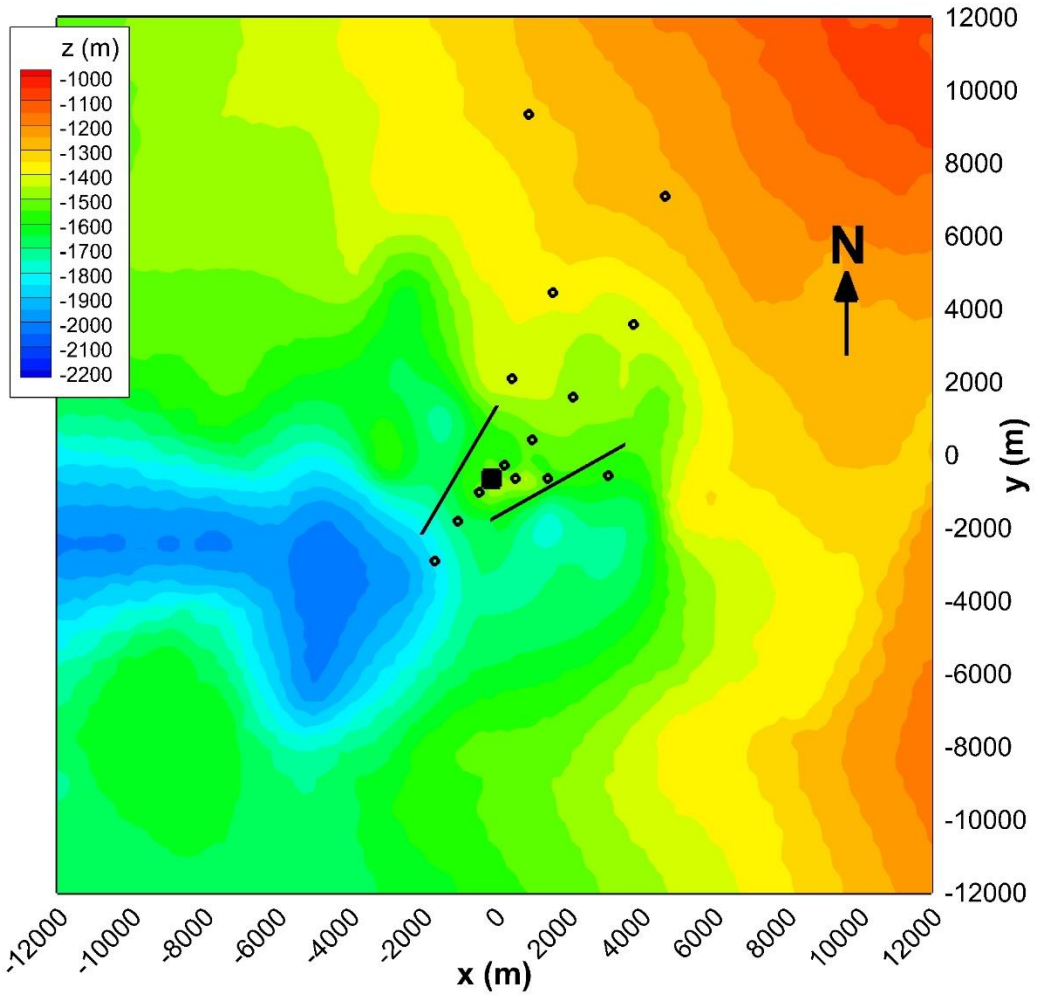

Figure 3. Elevation of the top of the storage formation assuming ground surface is at z = 0 m. The injection well (black square) is NE of a deep pendant of the caprock (blue region). Buoyancy is expected to carry CO_2 to the NE toward the yellow and reddish colored attics of the reservoir.

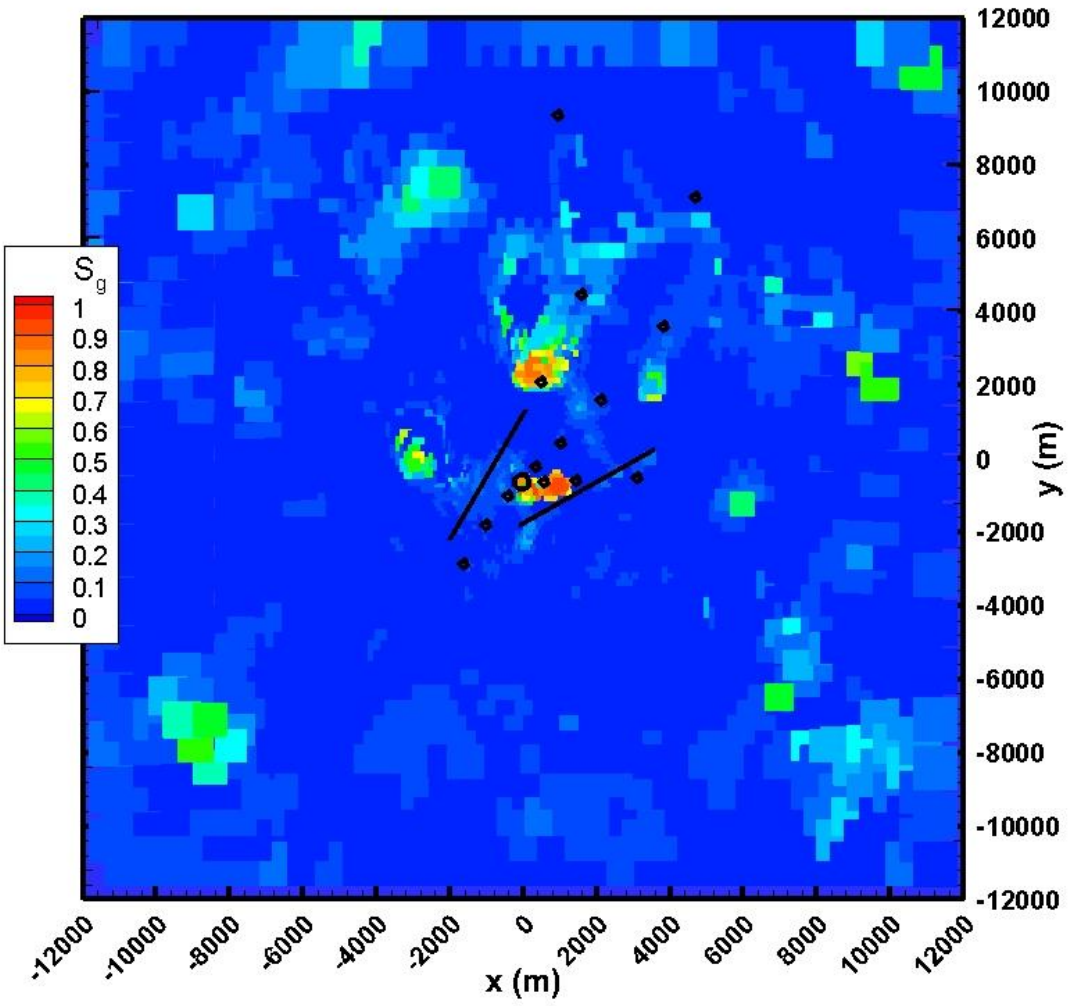

Figure 4. Initial saturation conditions in the actual model showing free-phase CH_4 localized in attic regions by buoyancy forces.

Injection and Monitoring Scenario

The scenario simulated specifies 8 Mt/yr of CO_2 injection for 20 years, and we run the simulation out another 180 years to observe very long-term evolution. Injection is into the lower half of the storage reservoir allowing for buoyant rise of injected CO_2 up into the attic regions of the reservoir. Studies such as Foxall et al. (2017) found that in highly permeable California Delta sandstones, one well was sufficient to inject at this rate (i.e., near-well pressure remains below

195 frac pressure). The injection well and 14 monitoring wells are included in the model to serve as
196 points in the system where measurements of pressure, saturation, and gas composition are
197 assumed to be made over time (Figure 2). At the injection well (I) and at nine nearby monitoring
198 wells (D, L, U wells, named for their general locations downstream, lateral, and upstream
199 relative to the injection well), we assume monitoring is done at two depths: (1) top of the
200 perforated interval, and (2) top of the storage reservoir. At five more-distant wells (F wells,
201 named for being far from the injection well), we assume monitoring is done only at the top of the
202 storage reservoir. The total number of monitoring wells assumed here is probably unrealistically
203 large (i.e., more than would be installed in any actual project, especially in the early stages of
204 injection), but for this simulation study we need good spatial coverage to demonstrate how
205 pressure and saturation change in the system for the entire project period. While pressure is
206 assumed to be available continuously, saturation measurements (e.g., obtained using a pulsed
207 neutron logging technique such as Schlumberger's time-lapse Reservoir Saturation Tool (RST))
208 and fluid sampling to measure gas- and liquid-phase composition, e.g., by U-Tube sampling
209 (Freifeld et al., 2005), could be carried out at discrete times. Although not used for the present
210 study, continuous temperature measurements are straightforward to make, and would likely be
211 part of any monitoring dataset at GCS sites.

212 ***3.2 Operational Model System***

213 It is important to remember that the model described above was created to generate the synthetic
214 data (i.e., describing the actual system) that will be compared to a series of subsequent models.
215 We will refer to the two classes of models as the actual model and the operational model,
216 respectively. The operational model is developed to mimic the kind of model that operators of
217 the site would use to design the injection scenario, design monitoring plans, estimate Area of

Review (AoR), obtain their injection permit(s), and manage ongoing operations. The first operational model is based on data available prior to injection. Moreover, the first operational model and its early updates may be developed based on subsets of all of the monitoring wells that are ultimately installed (i.e., early operational models will be developed prior to all of the wells being installed), again resulting in reliance on a limited set of data. In general, the operational model will be simpler and more generalized early in a project and become more detailed and accurate later in the project. The present study is aimed at demonstrating such improvement and corresponding reduction in uncertainty of model results and forecasts.

The operational model utilizes the same grid and boundary conditions as the actual model. But we assume that early in the project the operators would simplify the reservoir system and assume it to be homogeneous. Furthermore, complexities like hysteresis in relative permeability and capillary pressure would likely be omitted due to lack of data. Similarly the inclusion of residual CH_4 in the system is a complication that would likely be left out for simplicity in early operational models. In Table 1, we summarize the properties of the actual and operational models. The years at which various features were added to the operational models are also shown; the rationales for these additions are described in the next section.

234 *Table 1. Properties of the actual model and the initial operational model.*

Model Feature	Actual Model	Initial Operational Model	When Features Added
Formation Geometry	From geologic model: dipping storage formation about 500 m thick; lateral extent: 47 km by 60 km; undulating caprock/formation interface	Same as Actual Model	Year 0 (initial)
Lateral Boundary Conditions	Three closed lateral boundaries represent sealing faults, open updip lateral boundary represents transition to a shallower aquifer system	Same as Actual Model	Year 0 (initial)
Layering	20 layers from well log, range of ϕ: 0.24 – 0.35, range of k_h: 3.7 – 551 mD, range of k_v: 0.008 – 188 mD	No layers: uniform ϕ = 0.3, k_h = 24 mD, k_v = 1.2 mD	Year 1
Faults	Two vertical faults, k_h = 5 mD, k_v = 200 mD	No faults	1st fault -Year 2, 2nd fault -Year 10
Lateral Heterogeneity	Stochastic heterogeneity (GSLIB, Deutsch and Journel 1992); permeability roughly log-normal, conditioned to well log, range of ϕ: 0.025 – 0.56, range of k_h: 0.015 mD – 68 D, log-mean k_h =22 mD; range of k_v: 0.014 nD – 63 mD	None	
Multi-phase flow properties	Hysteretic van Genuchten (Doughty, 2007); S_{lr}, m, S_{grmax} depend on permeability: range of S_{lr} = 0.03 – 0.42, range of m: 0.86 – 1.25, range of S_{grmax} = 0.027 – 0.50; Leverett scaling for P_{c0}	Non-hysteretic van Genuchten (1980): S_{lr} = 0.116, m = 1.052, S_{gr} = 0 during injection period; S_{gr} = 0.2 during post-injection period	Year 25, Year 50
Initial Conditions	Hydrostatic pressure distribution, geothermal temperature gradient, gas-phase CH_4 in localized attics up against lower-most caprock	Same but no CH_4	Year 5

235

4. Results

4.1 Actual Model

Complete information

Figure 5 shows layer and cross-section views of the CO_2 plume at the end of the injection period, 20 years, and at the end of the extended simulation at 200 years. Note that CO_2 moves readily upward in the formation from the perforated interval to the top of the formation. As the CO_2 plume develops, it is surrounded by a halo of free-phase CH_4, which forms when CH_4 dissolved in the brine exsolves into the gaseous phase provided by the injected CO_2 (e.g., Oldenburg et al., 2013).

Figure 6 shows the maximum pressure change in the uppermost layer of the storage formation which occurs at the end of the injection period. The black contour line indicates a pressure change of 1 bar, which would be sufficient to lift fluid 10 m.

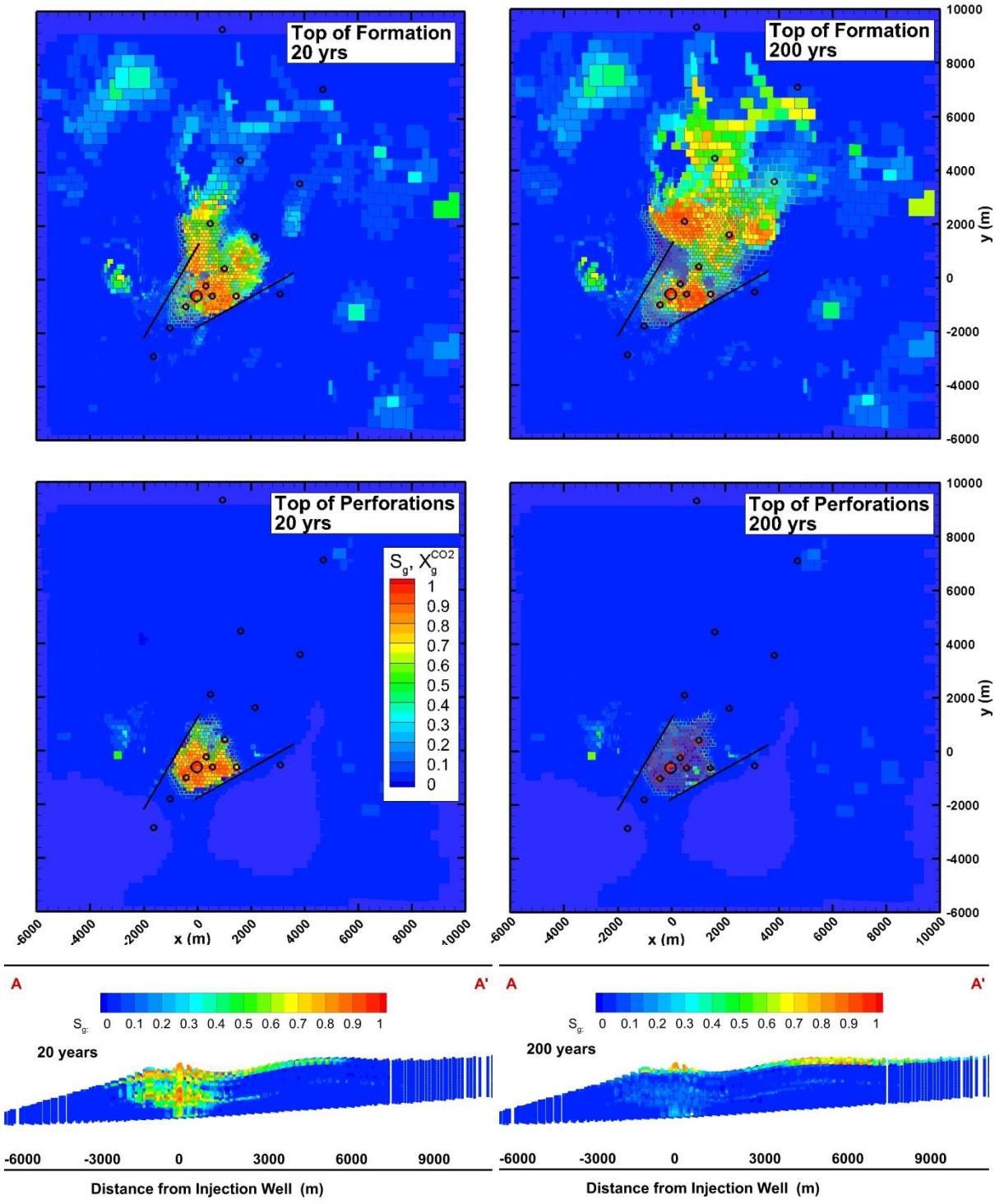

Figure 5. Distribution of CO_2 at the end of the injection period (left column) and at the end of the simulation (right column). In the top four frames, the cell fill color indicates gas saturation and the cell outline color indicates CO_2 mass fraction. The location of the cross-sections is shown in Figure 2.

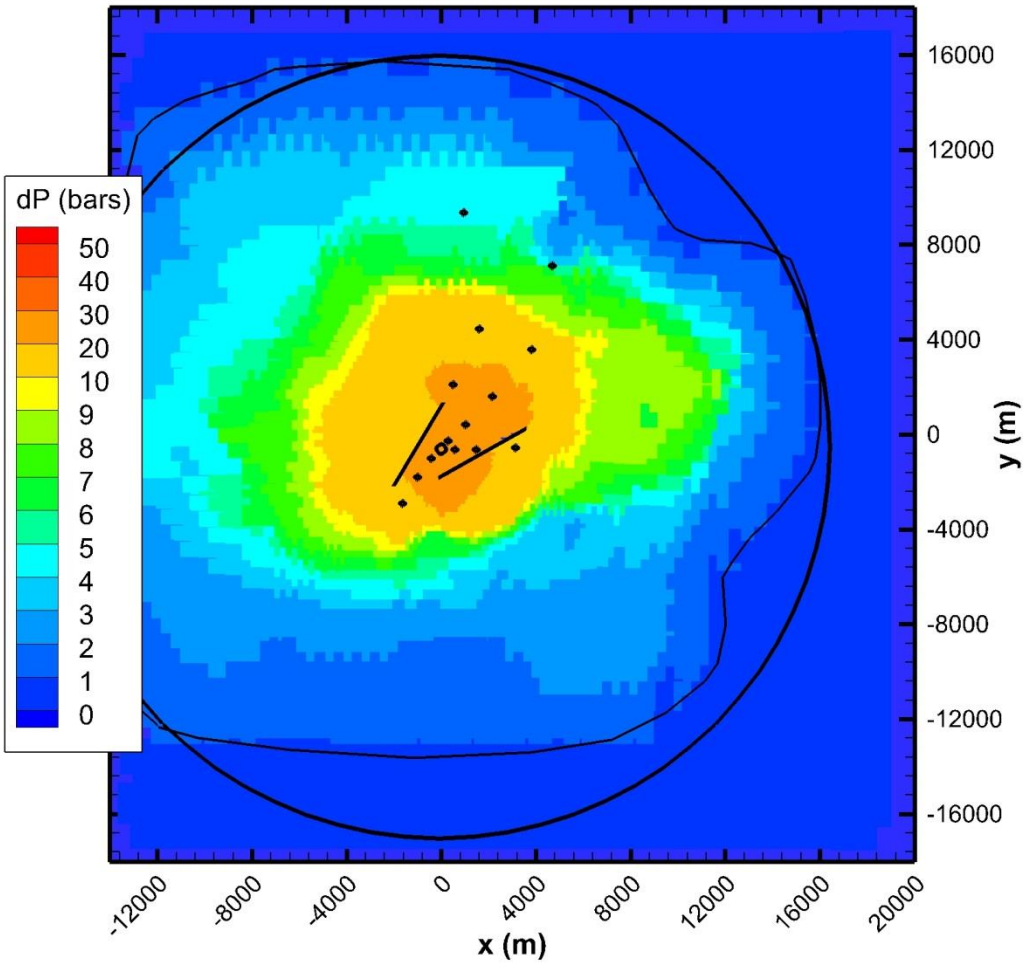

256

257 *Figure 6. The layer at the top of the storage formation, showing the pressure increase at the end*
258 *of the injection period. The thin black line outlines the region with dP > 1 bar and the thick*
259 *black line approximates this region with a circle of radius 16.5 km.*

260 ## Monitoring Data

261 Figures 5 and 6 provide a complete view of the evolution of the CO_2 plume and pressure pulse,

262 but we will not use these data in operational model development. Rather, to demonstrate the

263 evolution of conformance uncertainty over time, we limit ourselves to monitoring data that

264 would be obtained from monitoring wells consisting of pressure transients (Figure 7) and

265 saturation profiles (Figures 8 and 9). Moreover, we do not use the entire 200-year duration of

266 these data, but just the portion up to the year in which the model development is occurring. All
267 wells show pressure changes very soon after injection starts (Figure 7), but saturation changes
268 occur later at more distant monitoring wells (Figure 8). The sequence of saturation changes at the
269 injection well (Figure 9) is typical of the nearby monitoring wells, in that the first response is at
270 the depth of the perforated interval, with upward movement of the CO_2 plume occurring later
271 during the injection period and continuing through the full simulation period. In contrast, in more
272 distant monitoring wells, the CO_2 plume arrives in the uppermost portion of the storage
273 formation and stays there at all subsequent times.

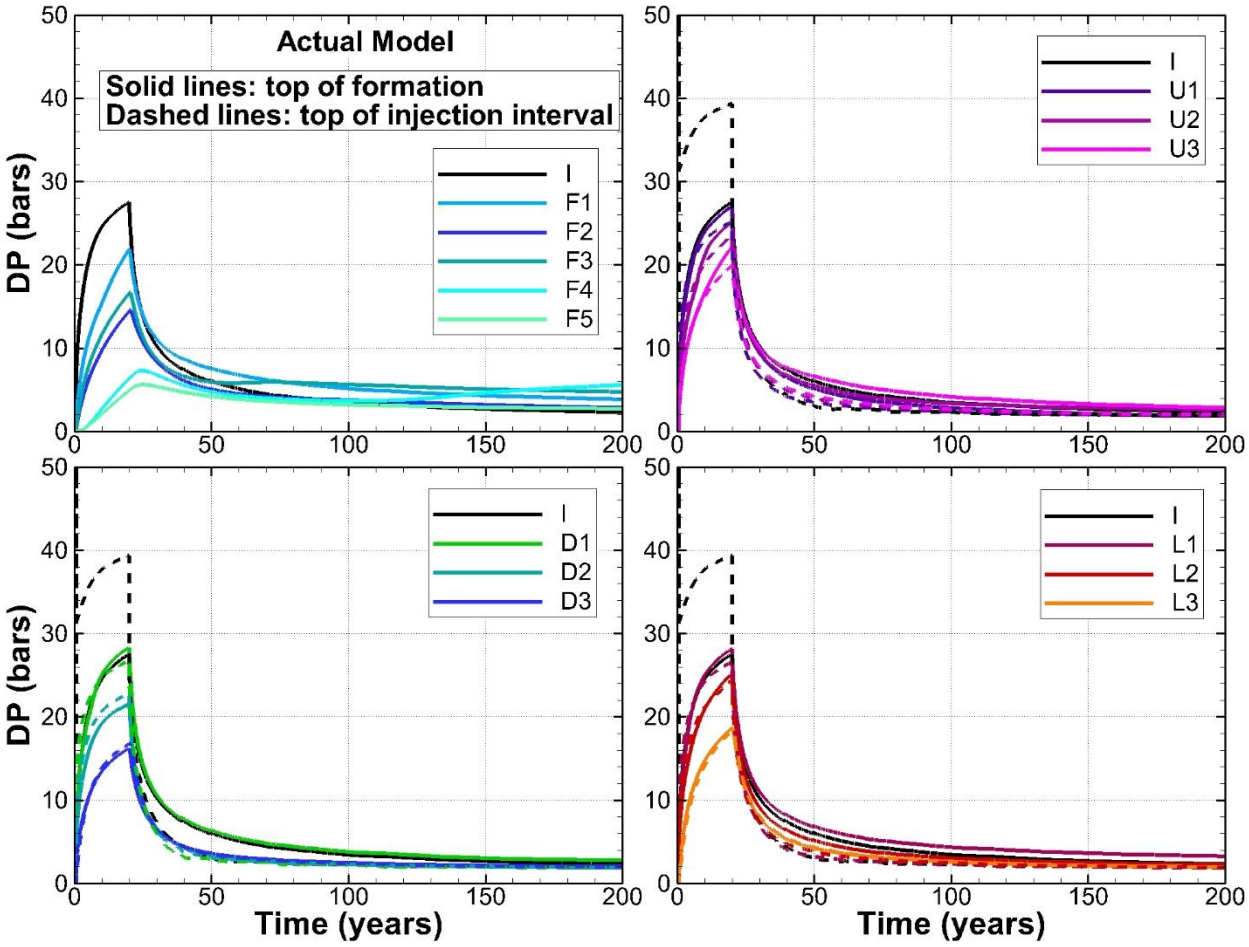

Figure 7. Actual model pressure transients. Legends show well names; see Figure 2 for locations. The upper left frame shows the far wells, and the other three frames show the U, D, and L wells. The injection-well response is shown in each frame for reference. Dashed and solid lines show the response at the top of the perforated interval and the top of the storage formation, respectively.

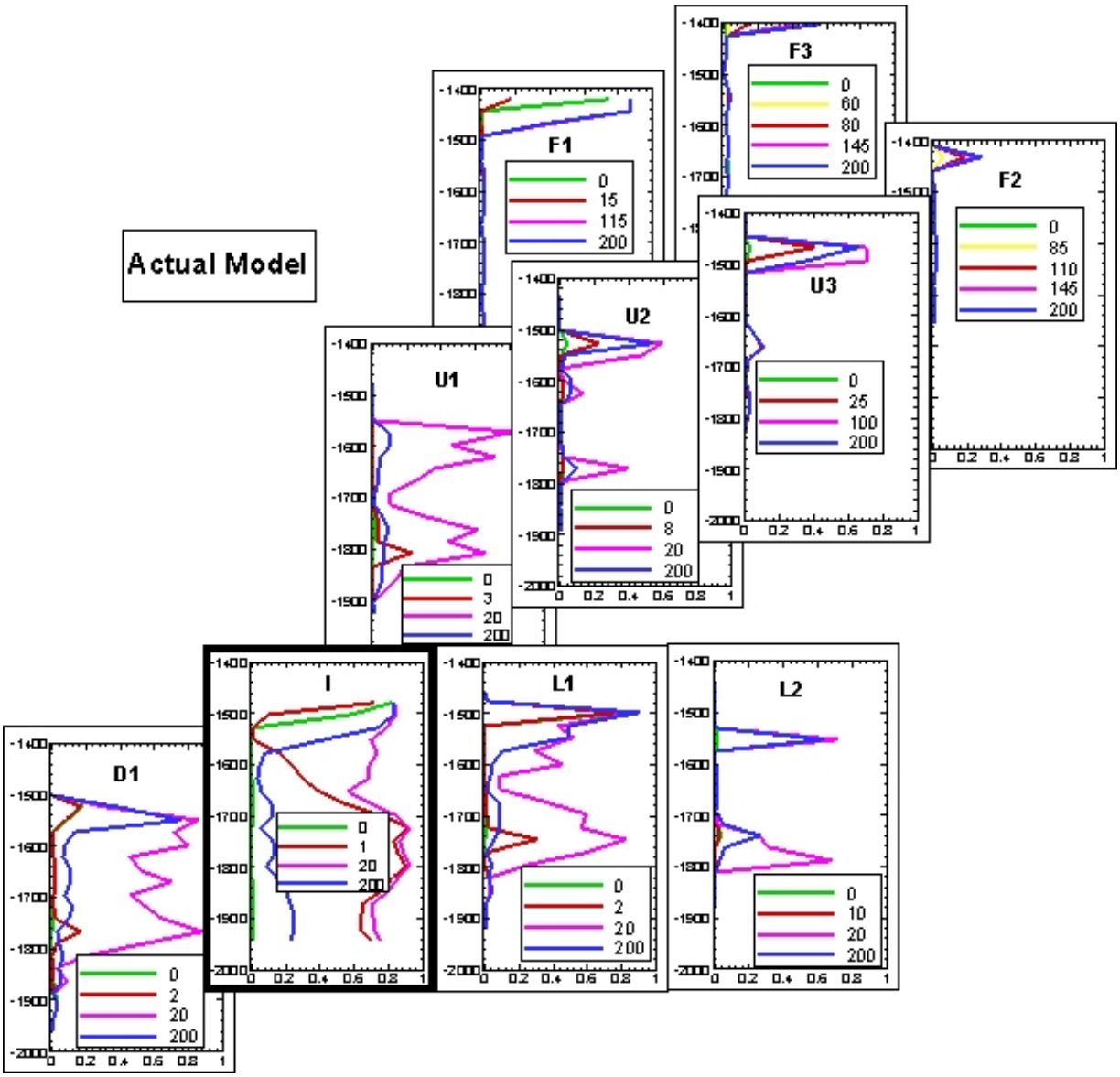

Figure 8. Selected saturation profiles in the monitoring wells for the actual model: green is the initial condition (gas is CH_4), yellow shows first increase in CH_4, red shows first increase in CO_2, pink is the maximum S_g, and blue is the final condition at 200 years. Of the 15 wells available for monitoring, saturation changes are only observed in these 10 wells. X axis is gas saturation S_g; Y axis is depth in meters; legend is profile time in years. The layout of profile plots corresponds to well location (Figure 2).

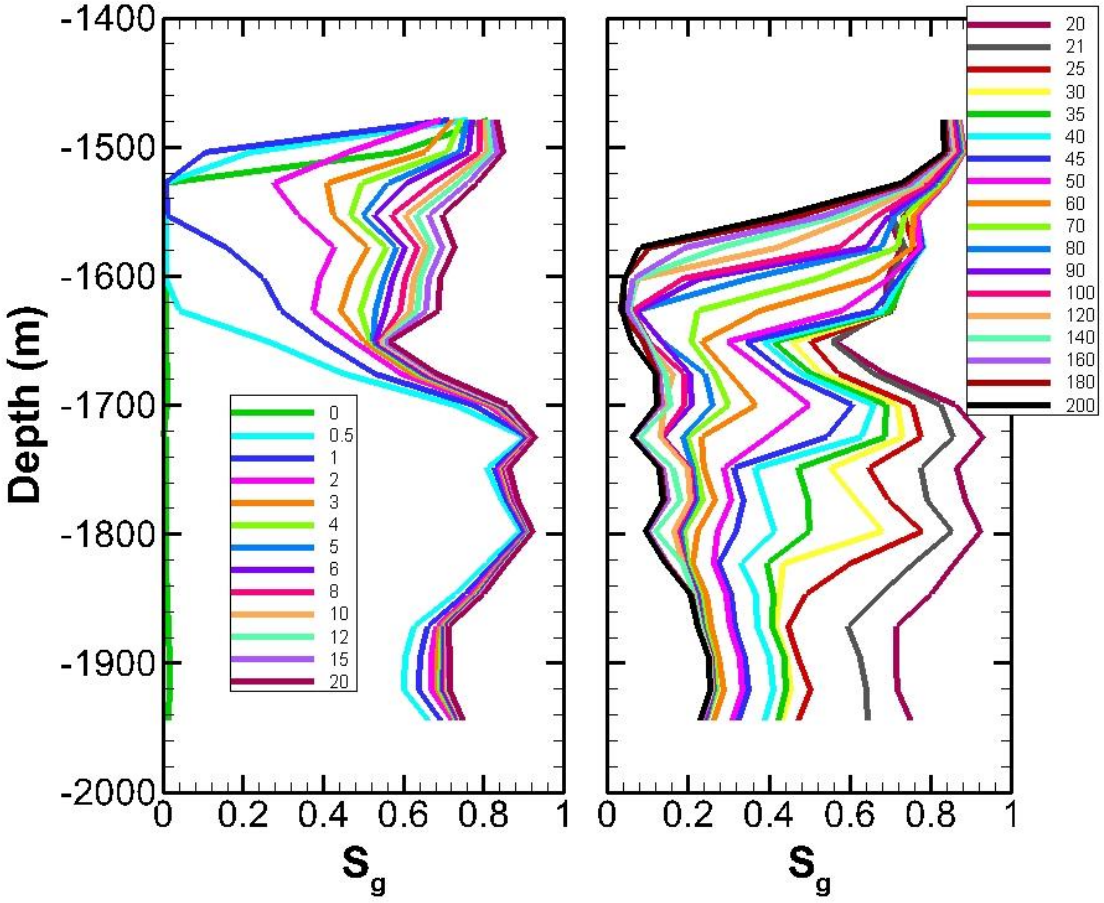

Figure 9. All saturation profiles in the injection well for the actual model. The legend numbers indicate profile time in years. The left-hand-side frame shows times during the injection period and the right-hand-side frame shows times during and beyond the 50-year PISC period. Colors are arbitrarily chosen to enhance profile visibility.

Metrics for comparing models

The two key metrics we use to judge concordance between the actual model and the operational models are (1) the extent of the CO_2 plume updip migration at the end of the 200-year simulation period, denoted R_0, and (2) the extent of the pressure pulse at the end of the injection period, denoted R_1, as inferred from monitoring well data. Figure 10 shows R_0 as a function of time for the actual model. Each symbol shows the time at which the CO_2 plume arrives at a monitoring well, quantified as a minimum gas saturation of 0.02 and a minimum CO_2 mass fraction of 0.02.

Figure 11 shows the maximum pressure change at the monitoring wells at the end of the injection period, and R_1, taken from Figure 6. The pressure profiles are plotted against distance R from the injection well, and also against $R^{1/2}$. The goal is to use just the points taken from the monitoring wells, and extrapolate to estimate R_1. Plotting dP versus R does not enable a good extrapolation; a polynomial fit yields a very inaccurate estimate of R_1. Plotting dP versus $R^{1/2}$ does much better, allowing a linear fit that yields a reasonable estimate of R_1. This provides a recipe for determining the extent of the pressure pulse for the operating models using only monitoring well data.

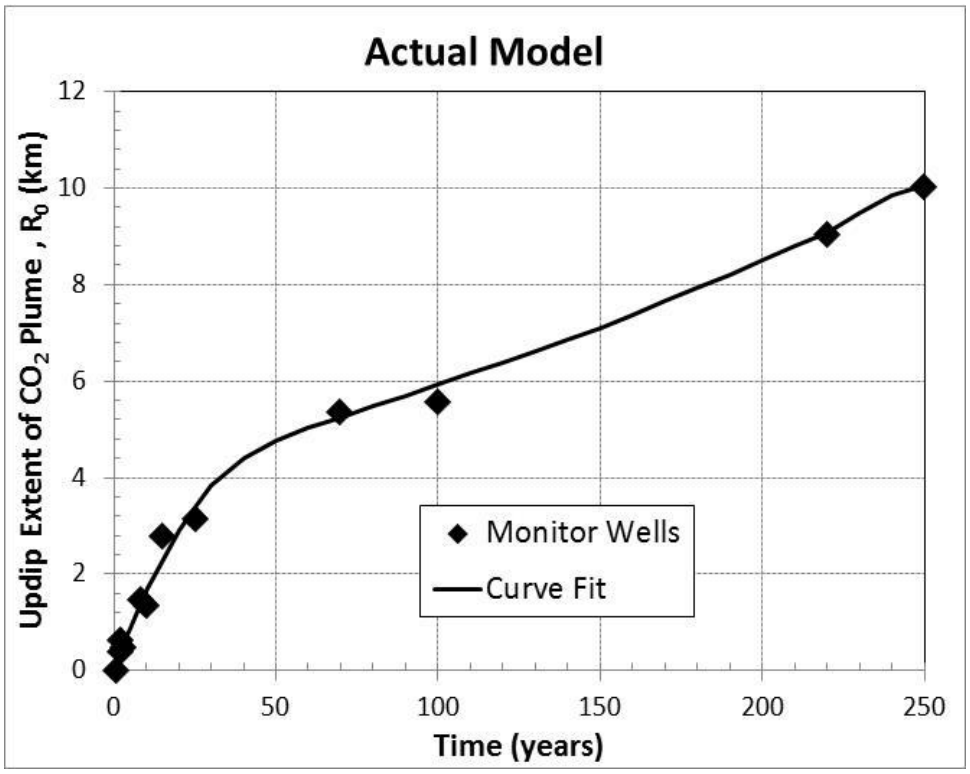

Figure 10. Up-dip extent of the CO_2 plume, R_0, for the actual model.

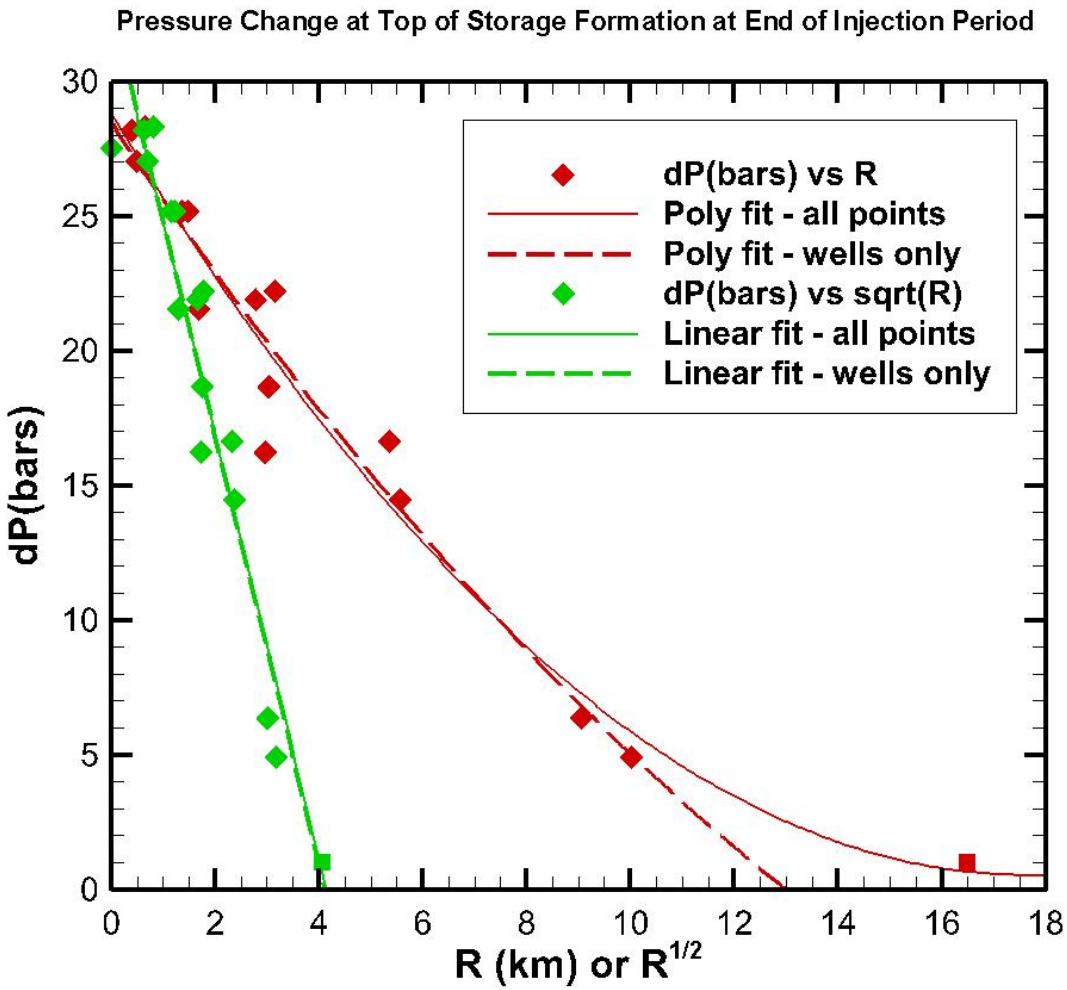

Figure 11. Actual model results: red diamonds: maximum pressure change at monitoring wells at the end of the injection period, plotted against distance from the injection well, R; green diamonds: maximum pressure change at monitoring wells plotted against $R^{1/2}$. Squares show $P(R_1) = 1$ bar. Solid lines show best-fit polynomial (red) and linear (green) functions including monitoring well data and $P(R_1)$. Dashed lines show fits including monitoring well data only.

4.2 Operational Model Development

Table 2 shows a summary of operational model development. Further details are provided below.

Year 1

The actual model monitoring data for the first year are shown in Figure 12. Note that at one year all but the most distant monitoring wells show a pressure response, but only the injection well shows any change in saturation. At the perforated interval, saturation increase indicates the

growing presence of the injected CO_2. Near the top of the formation, the small saturation decrease indicates less CH_4.

The corresponding forecast results for the initial operational model are shown in Figure 13. For the operational model, which is homogeneous, the pressure increases for the injection well and nearby monitoring wells are far too large, whereas the pressure changes for more distant monitoring wells tend to be too small. Also, the difference between pressure change at the perforated interval and at the top of the storage formation tends to be too large. Together, these observations suggest that operational-model permeability should be increased. The operational-model saturation profile at the depth of the perforated interval is too uniform, and in particular saturation is too large in the deeper portion of the perforated interval, suggesting that variable-permeability layers should be used. The gradual increase in operational-model saturation above the perforated interval provides information on the vertical permeability there, which seems about right. Because CH_4 is not included in the operational model, the shallow S_g peak observed in the actual model is absent.

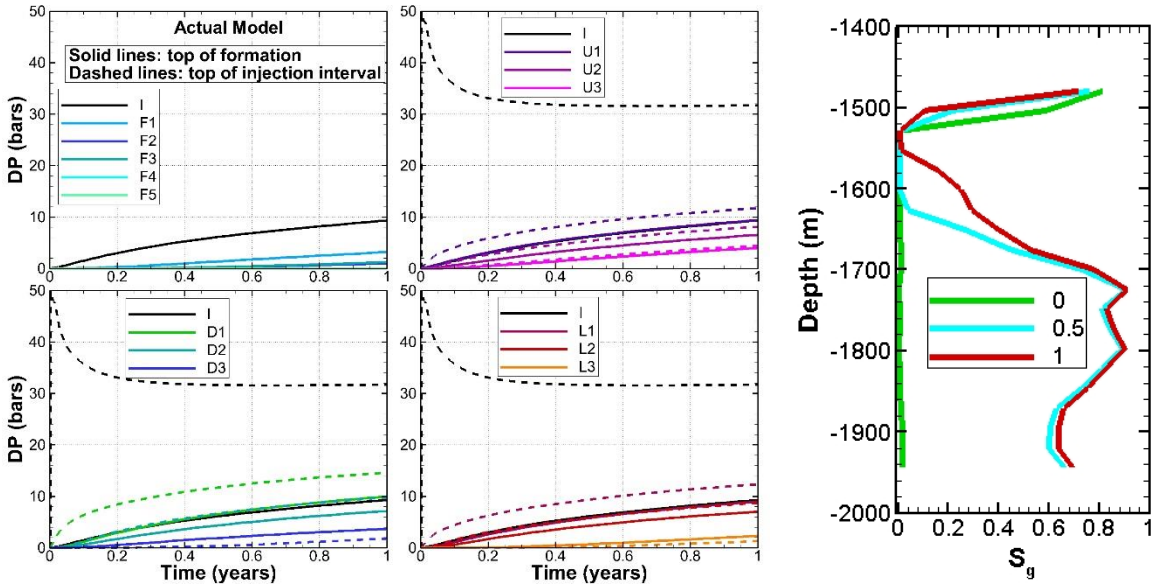

337

338 *Figure 12. Actual model Year 1 results. (left) pressure transients, (right) saturation profiles at*
339 *Well I.*

340

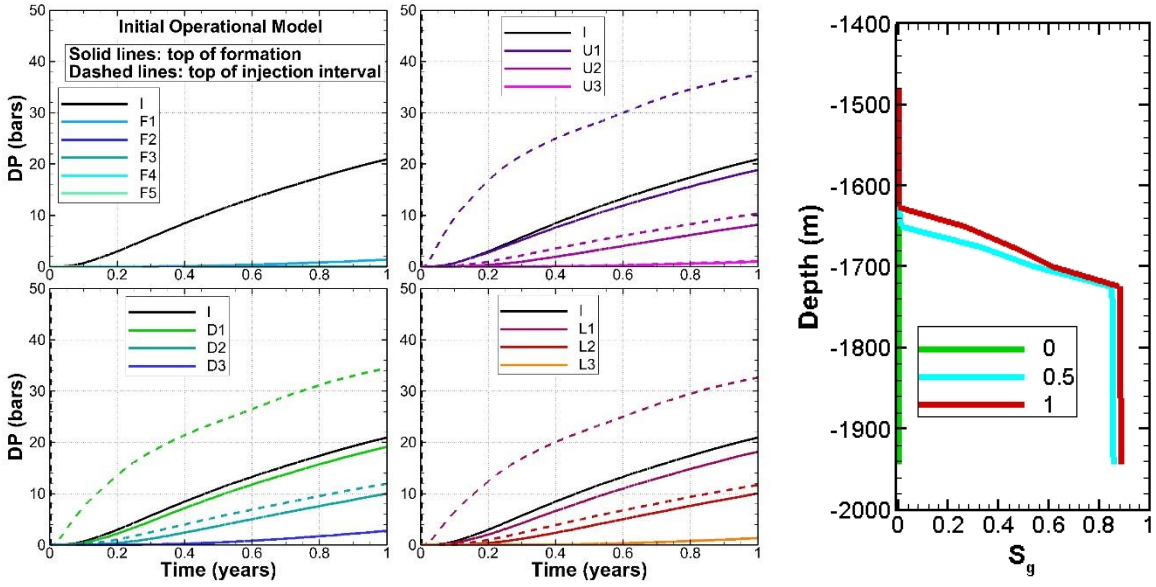

341

342 *Figure 13 Initial operational model Year 1 forecast: (left) pressure transients, (right) saturation*
343 *profiles at Well I. The pressure change at the perforated interval in the injection well is off scale*
344 *at about 100 bars.*

345 After several manual iterative updates of the operational model, including increasing overall

346 permeability and introducing a layered structure at the depth of the perforated interval, the final

one-year operational model hindcast results are shown in Figure 14. Horizontal permeability, which was uniform at 24 mD in the initial operational model, now varies from 3 to 121 mD over the perforated interval and is uniform at 121 mD above the perforated interval. Comparing Figures 12, 13, and 14 indicates that observations after one year allow updates to the operational model properties that greatly improve the pressure and saturation concordance to the actual model compared to the initial operational model, although most operational-model pressure responses are still a few bars too big.

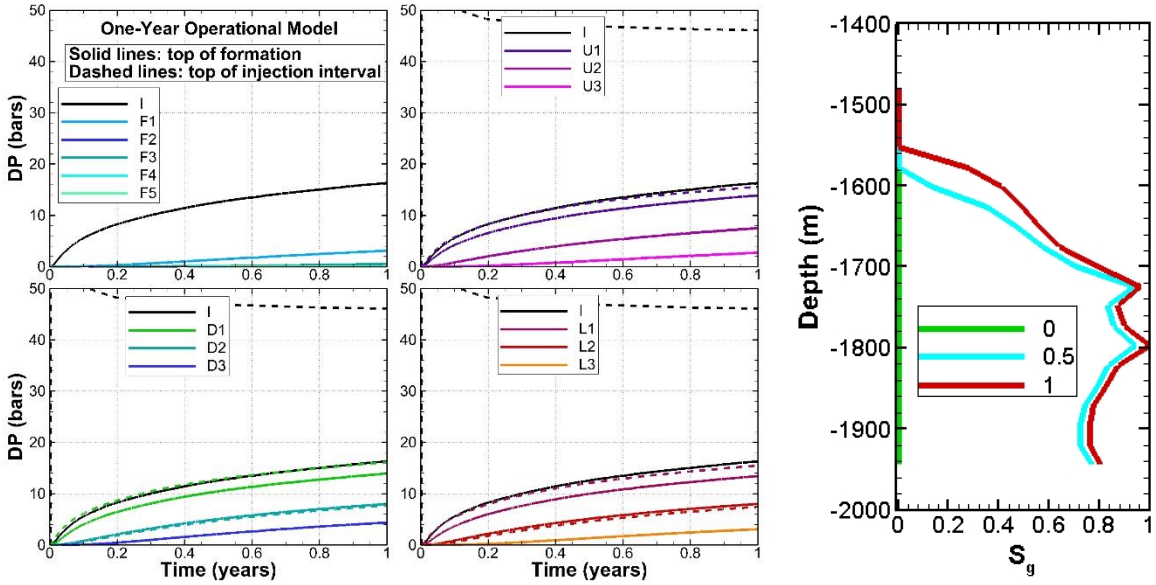

Figure 14. One-year operational model Year 1 hindcast: (left) pressure transients, (right) saturation profiles at Well I.

Year 2

The actual model monitoring data for the second year are shown in Figure 15. At two years the injection well and two nearby monitoring wells show saturation changes relative to initial conditions. The shallowest gas-saturation peak in each well represents attic gas (CH_4). The corresponding forecasts using the updated one-year operational model are shown in Figure 16. For the one-year operational model forecast for two years, the magnitude of the pressure change

in the injection well at the perforated interval is significantly too large (~47 bars compared to ~32 bars), but all the other pressure changes are within about 5 bars of the actual model. Note that the actual model shows a bigger separation between pressure response for Well L2 and Well L3 than does the operational model, suggesting that there should be a low-permeability zone separating the two wells. The operational-model saturation response at the perforated interval depth in Wells D1 and L1 is too small, suggesting that the variability of layer permeability should be larger. A small CO_2 peak in the actual-model injection-well saturation profile above the perforated interval suggests that a layered structure is needed for the shallow portion of the storage formation.

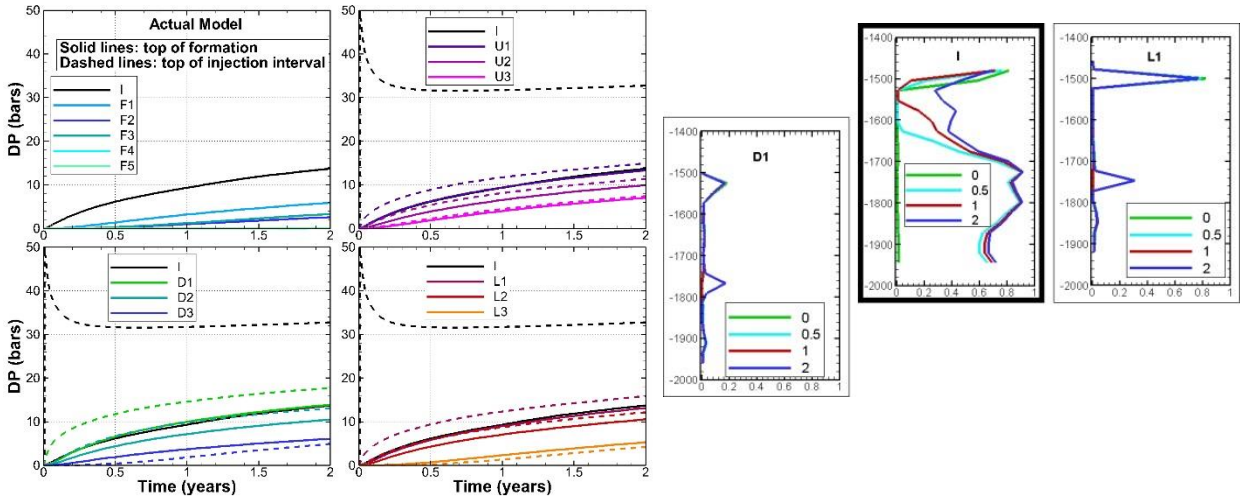

Figure 15. Actual model Year 2 results: (left) pressure transients, (right) saturation profiles.

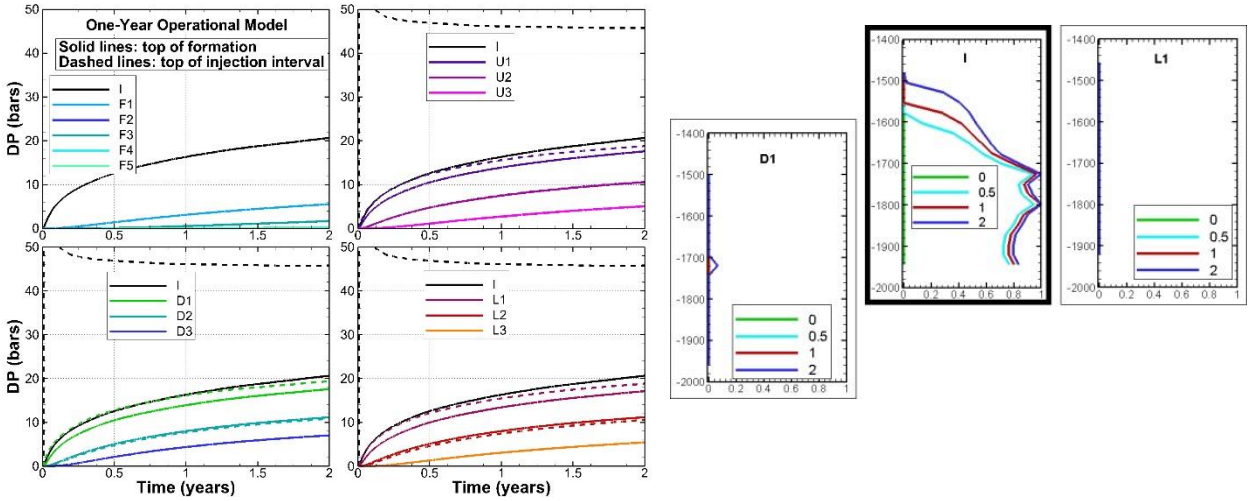

Figure 16. One-year operational model Year 2 forecast: (left) pressure transients, (right) saturation profiles.

After several model updates directed at improving the Year 2 concordance between actual and operational models, we set up a layered structure above the depth of the perforated interval, modified permeabilities at the perforated interval to encourage preferential flow, and introduced a fault between Wells L2 and L3. The final two-year operational model hindcast results are shown in Figure 17. Comparison of Figures 15, 16, and 17 indicates that the two-year operational model generally improves the concordance to the actual model compared to the one-year operational model. In particular, the final pressure change in the injection well at the perforated interval for the operational model is much closer to the actual value (~35 bars compared to ~32 bars), and the difference in pressure response between Wells L2 and L3 is larger, consistent with a low-permeability fault between them. The operational-model S_g peak arrival is still a little late in Wells D1 and L1, and a little early in Well U1, and the CO_2 peak developing above the perforated interval in Well I is not well represented. The shallow CH_4 peaks observed in Wells D1, I, and L1 in the actual model are absent in the operational model.

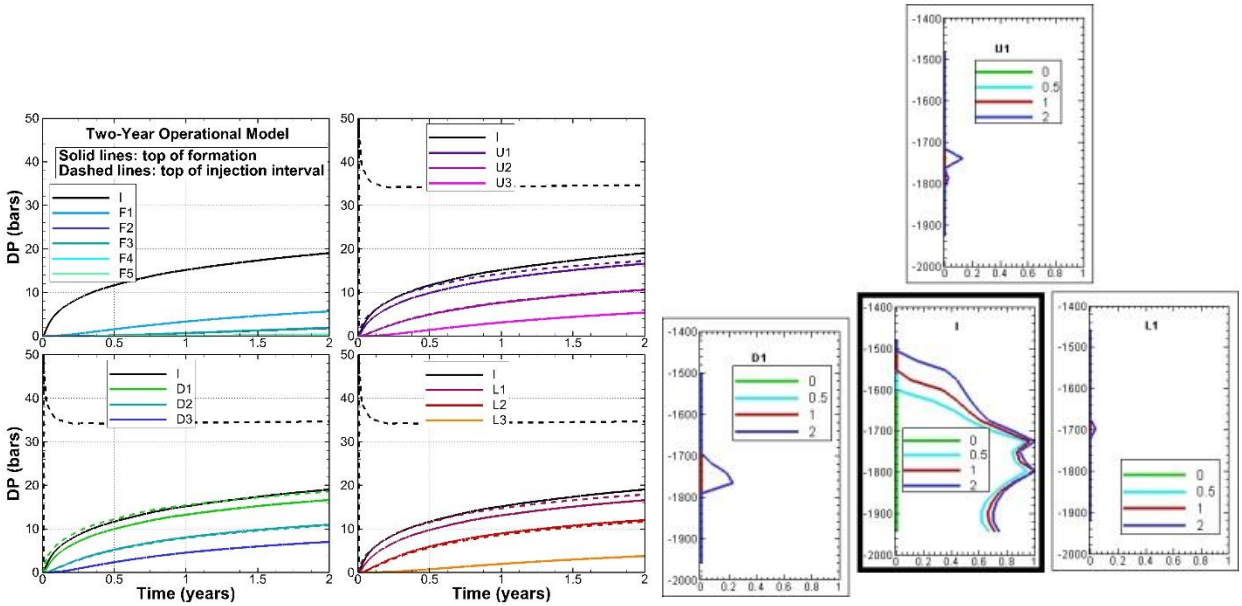

Figure 17. Two-year operational model Year 2 hindcast: (left) pressure transients, (right) saturation profiles.

Year 3

For brevity, we skip the description of the Year 3 comparison between actual and operational models. Table 2 summarizes the comparison, and details are provided in Doughty and Oldenburg (2019).

Year 5

The actual model monitoring data for the fifth year are shown in Figure 18—we skip Year 4 consistent with the idea that the frequency of model updating should decrease as understanding of the system increases. At five years the injection well and three nearby monitoring wells show saturation changes relative to initial conditions. The corresponding forecast results for the three-year operational model are shown in Figure 19. With a longer time period available for comparing pressure transients, by five years it is apparent that the operational model transients show too much curvature, i.e., they increase too rapidly at first, then level off too much later. After unsuccessful attempts to decrease curvature by increasing storativity by increasing rock

compressibility, it was decided that the presence of the additional gas phase in the form of a natural gas cap (CH_4) could provide the additional storativity needed. Thus CH_4 gas was added to the operational model in a pre-injection phase of model development in the same manner as the initial condition of the actual model was developed, i.e., by introducing it uniformly at a low saturation and allowing it to migrate upward into formation attic spaces during an initial gravity equilibration.

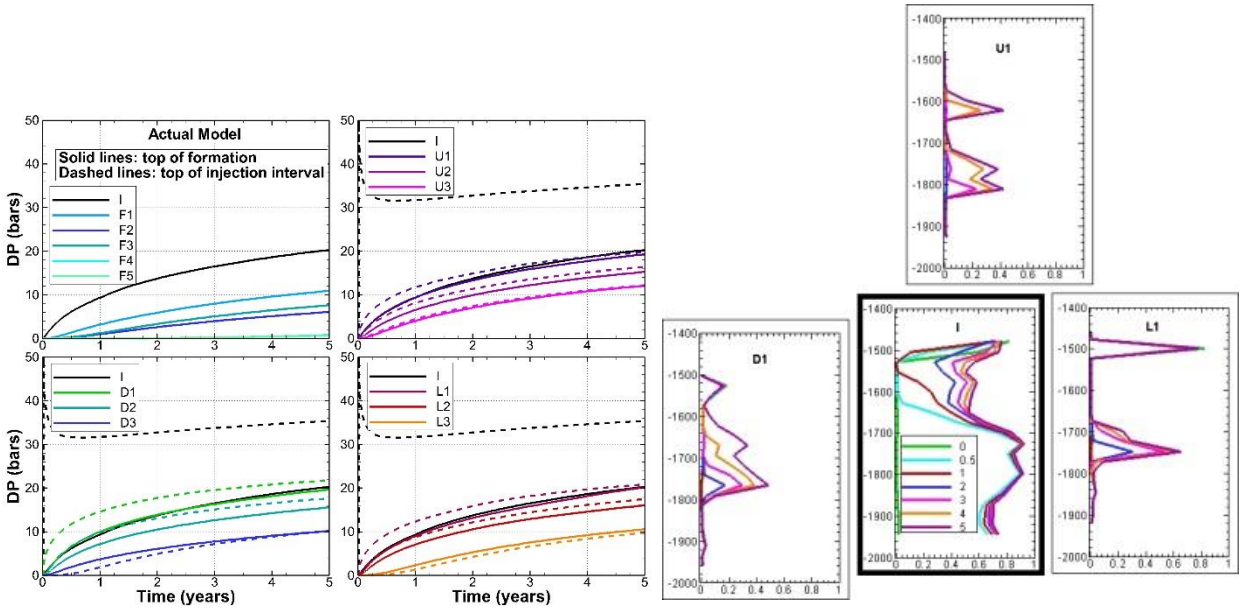

Figure 18. Actual model Year 5 results: (left) pressure transients, (right) saturation profiles.

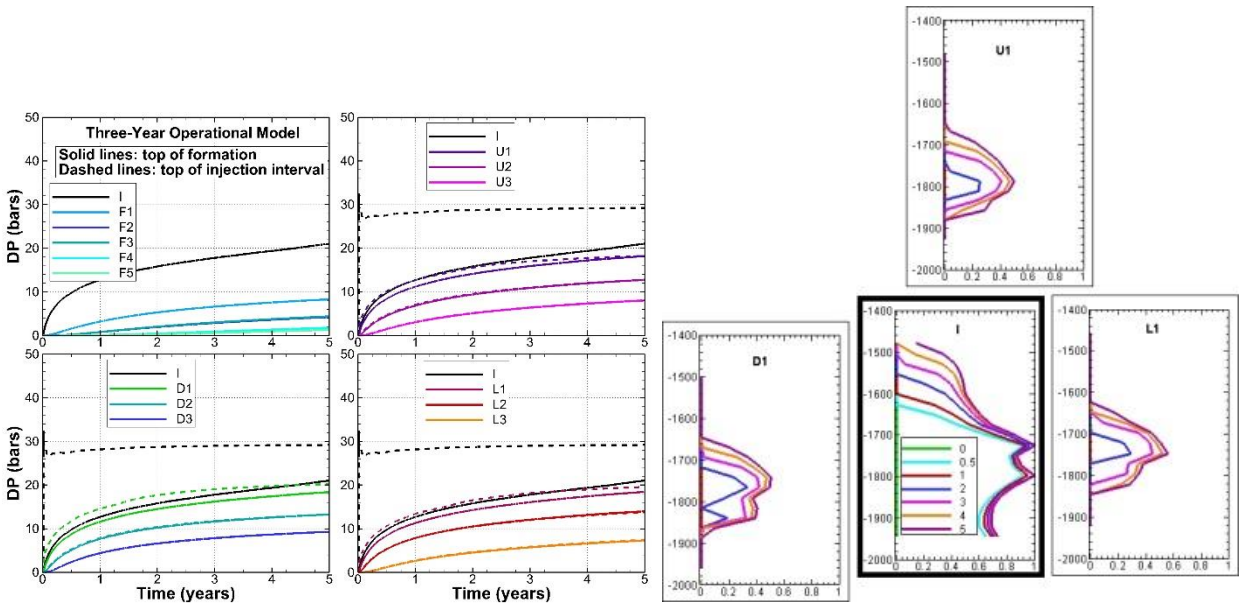

Figure 19. Three-year operational model Year 5 forecast: (left) pressure transients, (right) saturation profiles.

After several model update iterations, the final five-year operational model hindcast results are shown in Figure 20. The differences from the three-year operational model are the inclusion of CH_4 in the attic space and a decrease in the permeabilities just above the perforated interval. Comparing Figures 18, 19, and 20 indicates that the five-year operational model somewhat improves the concordance to the actual model compared to the three-year operational model. Compared to the three-year operational model, pressure changes are a little smaller in the injection well (which is now about 5 bars too small at the perforated interval) and nearby monitoring wells (which are now in better agreement with the actual model). Overall curvature of the *dP* versus time curve is only slightly better than before. Operational-model S_g peaks at nearby monitoring wells at the depth of the perforated interval, representing injected CO_2, are a little bigger, which is generally in better agreement with the actual model, and shallow S_g peaks showing CH_4 are now included.

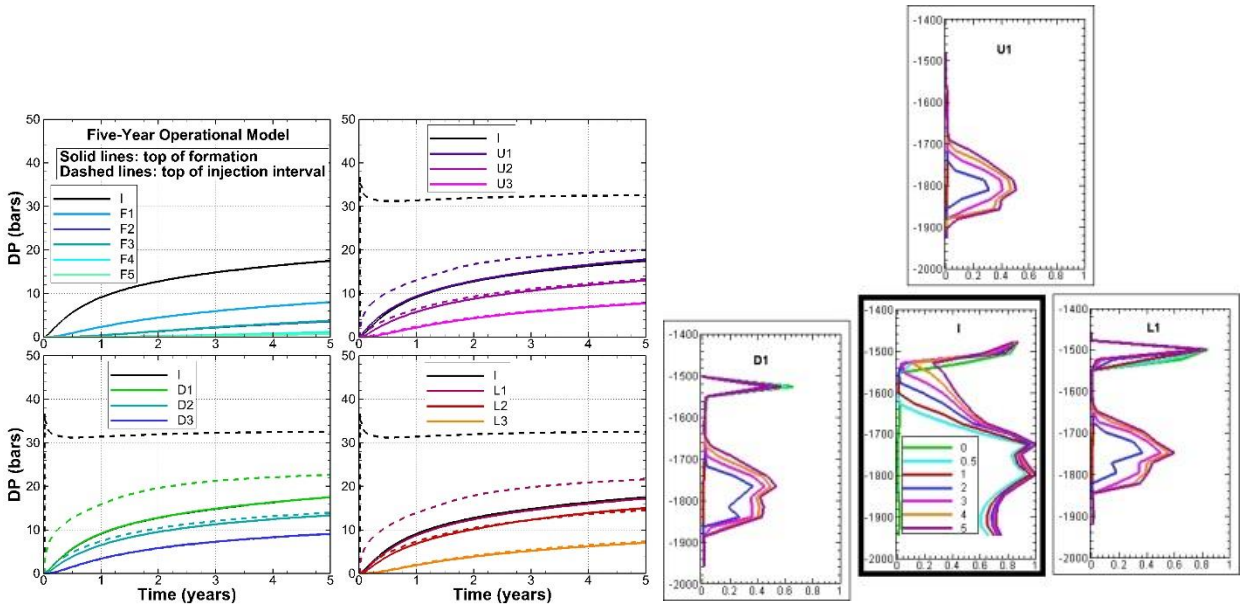

Figure 20. Five-year operational model Year 5 hindcast: (left) pressure transients, (right) saturation profiles.

Year 10

For brevity, we skip the description of the Year 10 comparison between actual and operational models. Table 2 summarizes the comparison, and details are provided in Doughty and Oldenburg (2019).

Year 20 – End of Injection Period

The actual model monitoring data for the 20th year are shown in Figure 21. At 20 years the injection well and six monitoring wells show saturation changes relative to initial conditions. The corresponding forecast results for the ten-year operational model run out to 20 years are shown in Figure 22. For the actual model all *dP* versus time curves are gradually increasing, but for the operational model they tend to increase too fast early, then level off too much late, showing too much curvature. This occurs more for the pressures at the depth of the perforated interval and is especially obvious at the injection well. However, the magnitude of *dP* is about right at 20 years.

In an attempt to get more gradually increasing pressure curves, the two faults were extended farther up dip, to create a more linear, less radial flow geometry. This is the only change made to create the final twenty-year operational model, and hindcast results are shown in Figure 23. The *dP* versus time curves show slightly less curvature. The saturation profiles for the ten-year and twenty-year operational models are very similar, and provide a reasonable concordance to the actual model.

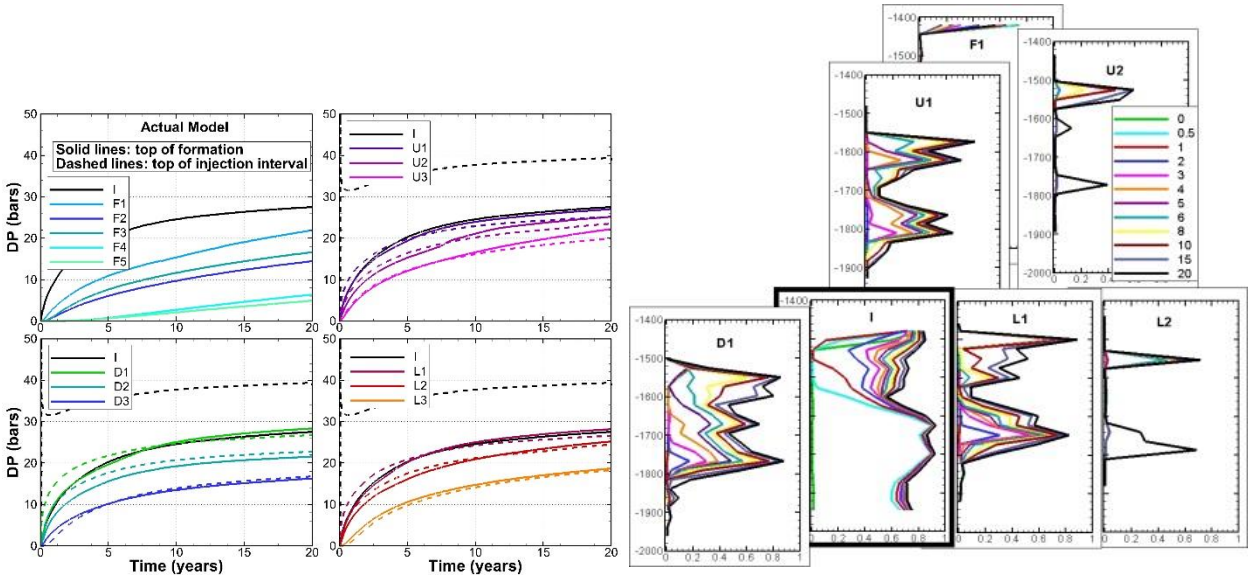

Figure 21. Actual model Year 20 results: (left) pressure transients, (right) saturation profiles.

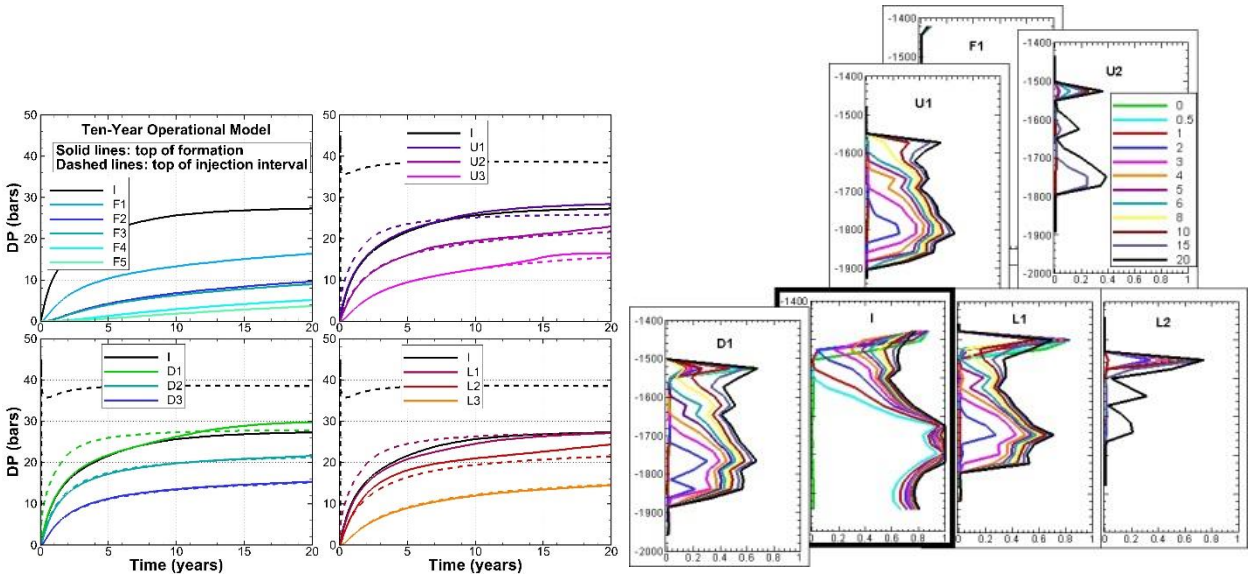

456

457 *Figure 22. Ten-year operational model Year 20 forecast: (left) pressure transients, (right)*
458 *saturation profiles.*

459

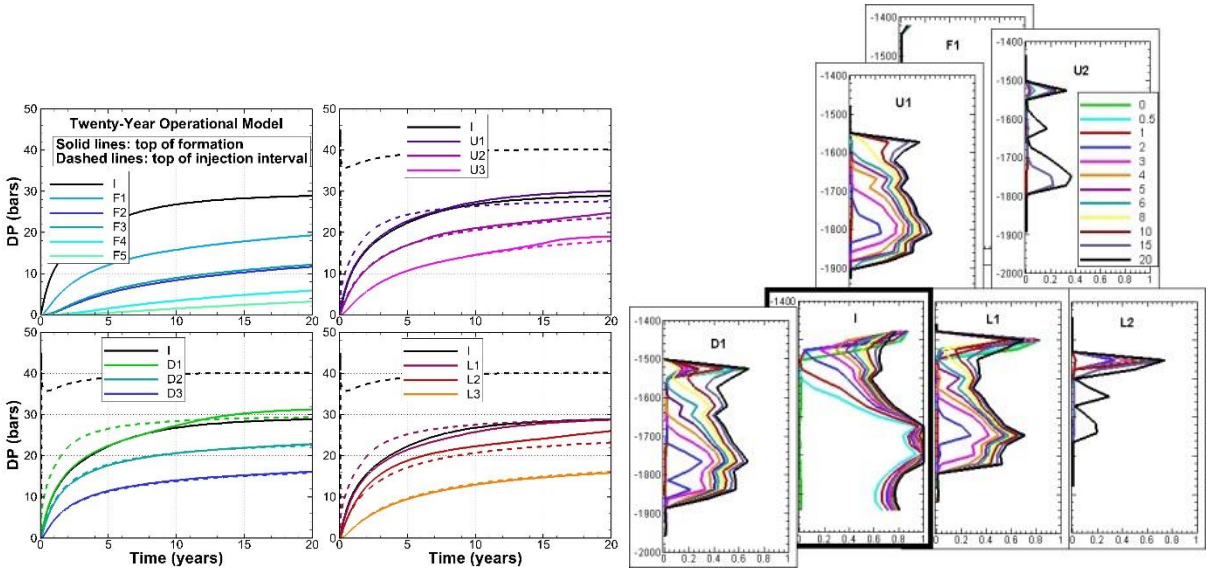

460

461 *Figure 23. Twenty-year operational model Year 20 hindcast: (left) pressure transients, (right)*
462 *saturation profiles.*

Year 25

The actual model monitoring data for the 25th year are shown in Figure 24. This is the first observation within the post-injection period. For clarity, only saturation profiles from the post-injection period are shown. After injection ends at 20 years, pressure change is decreasing in all wells except the two most distant monitoring wells, F4 and F5, where it is still increasing slowly. At 25 years the injection well and seven monitoring wells show saturation changes relative to initial conditions. Gas saturation is decreasing in the deeper portion of the formation and increasing in the shallow portion, as buoyancy flow acts to lift the CO_2 plume. The corresponding forecast results for the twenty-year operational model are shown in Figure 25. This is a non-hysteretic model with $S_{gr} = 0$ during the injection period and $S_{gr} = 0.2$ during the post-injection period.

By the end of the injection period, most of the *dP* values for the twenty-year operational model are too big, and the curvature of the *dP* versus time curve indicates too rapid a response for all wells, which is notable especially at the perforated interval of Well I, which flattens out too much towards the end of the injection period, and the far wells F4 and F5, for which *dP* does not continue to increase after injection ends. This suggests that the rock compressibility should be larger, to provide a generally slower response. Comparing the post-injection saturation profiles for the actual and twenty-year operational model shows that the gradual decline in gas saturation over the lower half of the reservoir, which occurs as CO_2 moves upward under buoyancy forces and water imbibes back into the pore space, is not produced by the operational model – S_g profiles change little between 20 and 25 years, indicating that this non-hysteretic approximation with $S_{gr} = 0.2$ for the post-injection period overestimates trapping of CO_2. After several iterations, the final twenty-five year operational model has doubled rock compressibility (0.3E-8

487 Pa^{-1} to 0.6E-8 Pa^{-1}), and two variations considered to better represent imbibition: a non-

488 hysteretic model with S_{gr} = 0 for the post-injection period and a hysteretic model. The hysteretic

489 model has a variable S_{gr}; during the injection period it remains zero nearly everywhere, and

490 during the post-injection period it varies spatially and temporally from zero to S_{grmax} = 0.2,

491 depending on the maximum value of S_g experienced by a given location. At the perforated

492 interval, where the maximum S_g during the injection period was near one, $S_{gr} \sim S_{grmax}$.

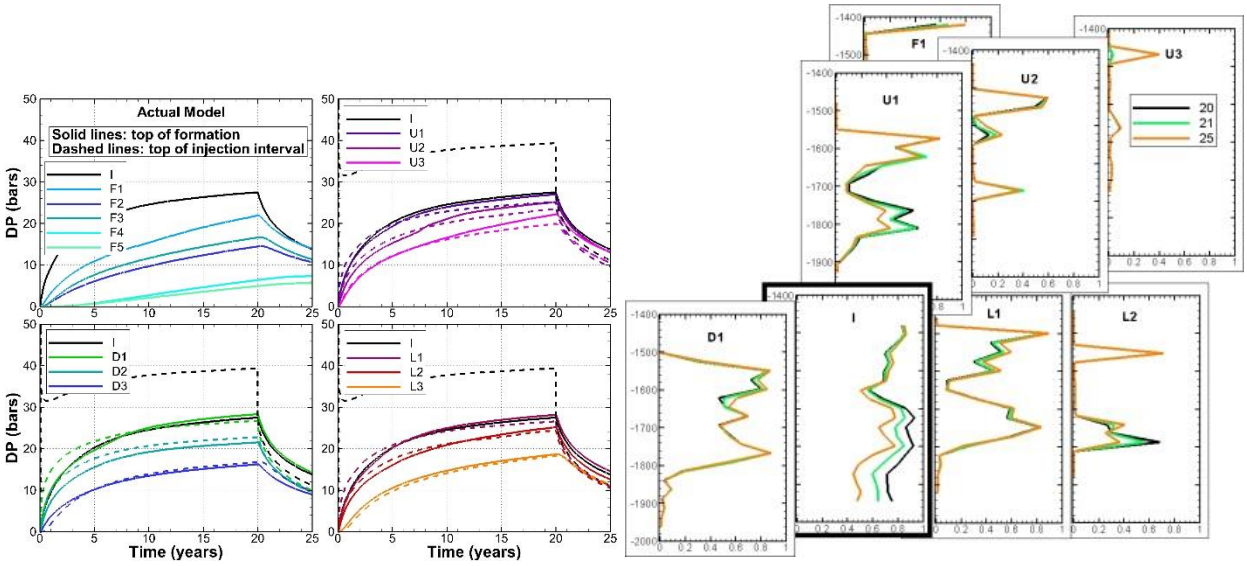

493

494 *Figure 24. Actual model Year 25 results: (left) pressure transients, (right) saturation profiles for*
495 *the first five years of the post-injection period.*

496

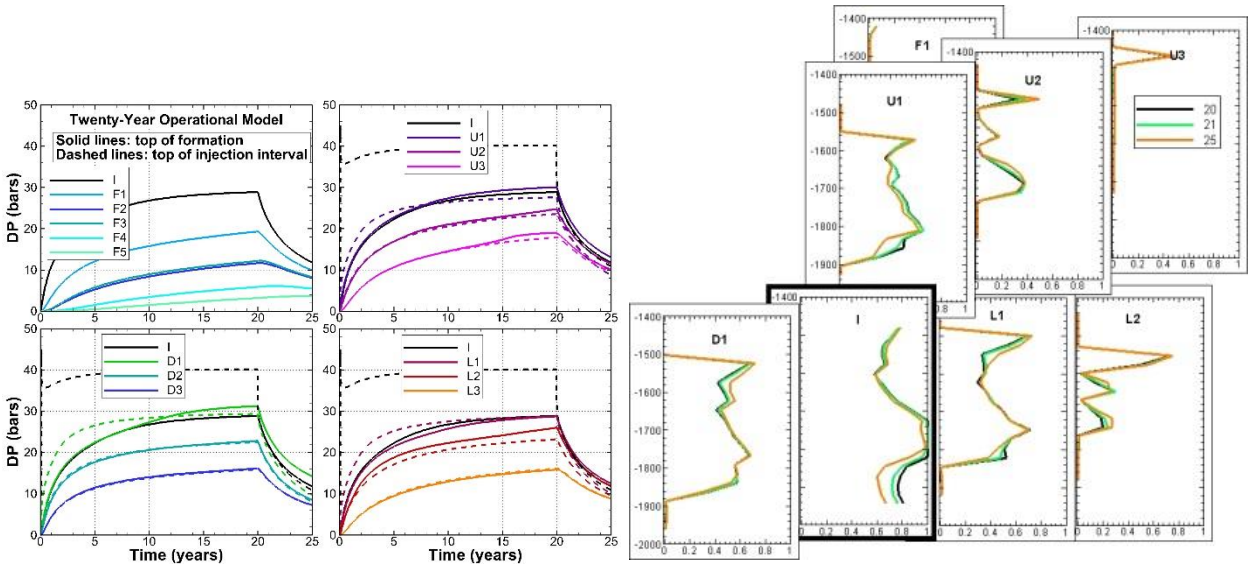

Figure 25. Twenty-year operational model Year 25 forecast: (left) pressure transients, (right) saturation profiles for the first five years of the post-injection period. Non-hysteretic model with S_{gr} = 0.2 during post-injection period.

The hindcast results for the saturation profiles for the twenty-five-year operational models are shown in Figure 26. Both the non-hysteretic and hysteretic operational-model saturation profiles now match the character of the actual model better, with more mobile CO_2 enabling a gradual gas saturation decline in the lower half of the reservoir and a gradual increase in the upper half. Pressure transients for the operational models (see supplemental material, Figure S4) are similar to those for the actual model.

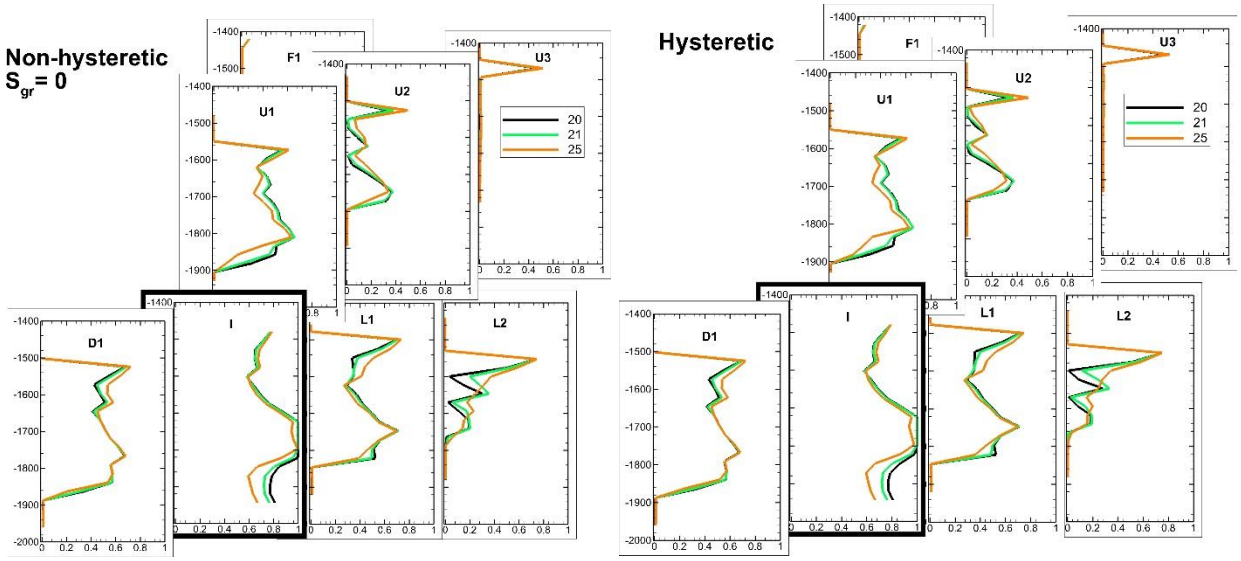

Figure 26. Twenty-five-year operational models Year 25 hindcast: saturation profiles for the first five years of the post-injection period: (left) non-hysteretic model and (right) hysteretic model.

Year 50

The actual model monitoring data for the 50th year are shown in Figure 27. At 50 years the injection well and seven monitoring wells show saturation changes relative to initial conditions. Pressure change is now decreasing in all wells. Gas saturation continues decreasing in the deeper portion of the formation and increasing in the shallow portion, as buoyancy flow acts to lift the CO_2 plume upward and updip in the storage formation. The corresponding forecast results for the saturation profiles for the twenty-five-year operational models are shown in Figure 28. Pressure transients for the operational models (not shown) are similar to those for the actual model.

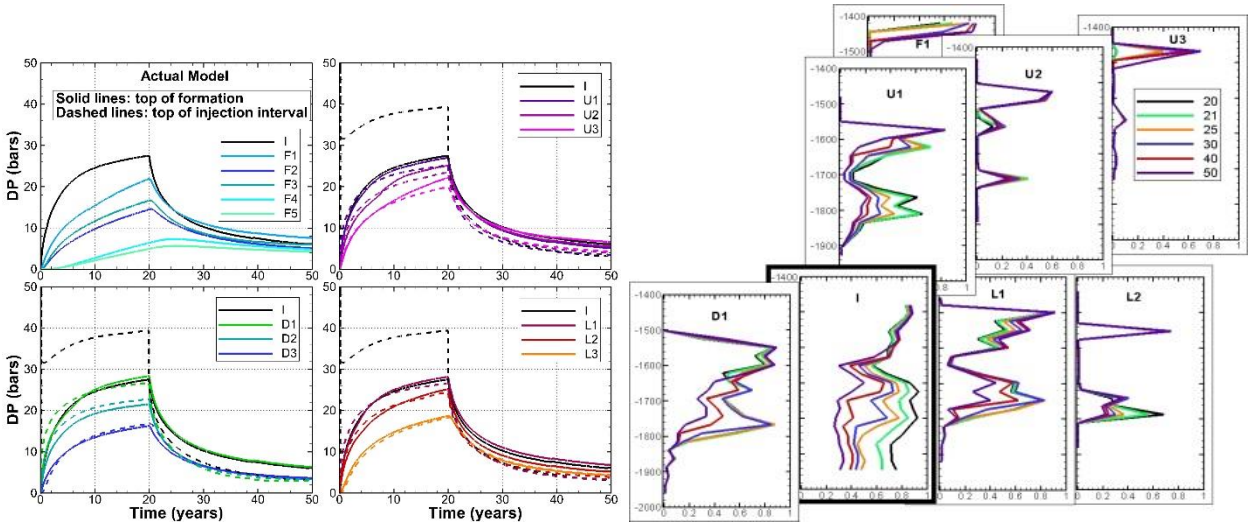

520

521 *Figure 27. Actual model Year 50 results: (left) pressure transients, (right) saturation profiles for*
522 *the first 30 years of the post-injection period.*

523

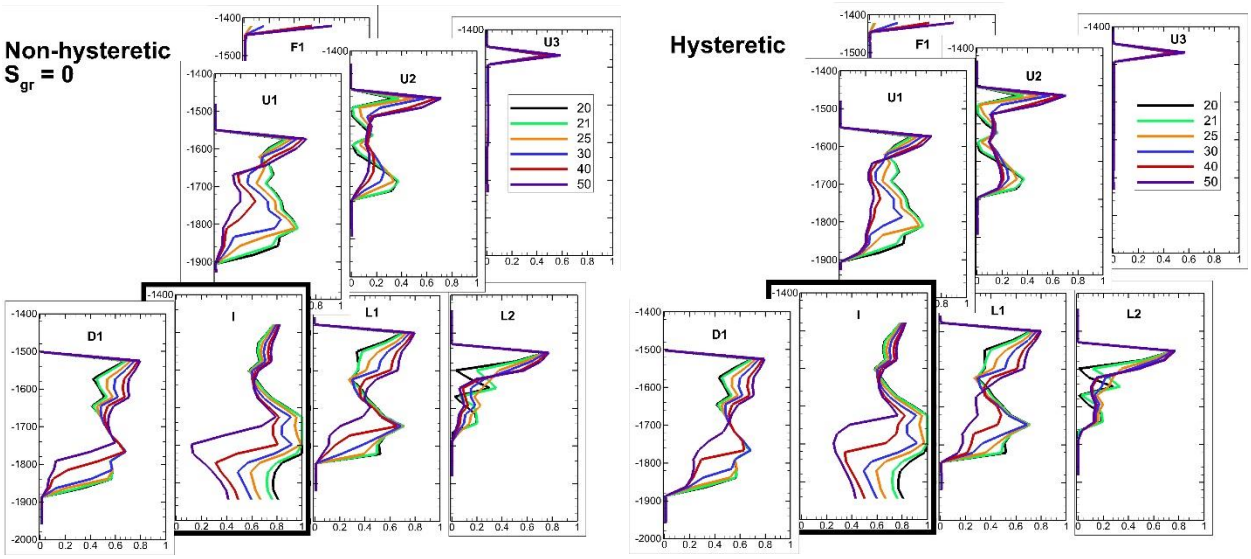

524

525 *Figure 28. Twenty-five-year operational models Year 50 forecast: saturation profiles for the first*
526 *30 years of the post-injection period: (left) non-hysteretic model and (right) hysteretic model.*

527 Comparison of the late-time saturation profiles in Figure 28 indicates that as S_g decreases, the

528 non-hysteretic model fails to show a convergence of S_g to 0.2 as the actual model (Figure 27) and

529 hysteretic operational model do. Hence only the hysteretic model is used for continued

530 operational model development.

Years 100, 150, and 200

The actual model monitoring data through the end of the PISC period at 70 years and on to 200 years are shown in Figure 29. Starting at 100 years, the injection well and nine monitoring wells show saturation changes. The corresponding forecast results for the fifty-year operational model are shown in Figure 30. The gradual decline in the *dP* versus time curves is similar in both models, but the actual model *dP* curves tend to plateau at 2-3 bars, whereas most of the operational model curves are about 1 bar lower. Both models show the saturation continuing to decline in the lower half of the formation, but at a slowing rate, as saturations approach residual saturation. The fifty-year operational model concordance to the actual data is deemed acceptable for 100, 150, and 200 years and no further model development is done.

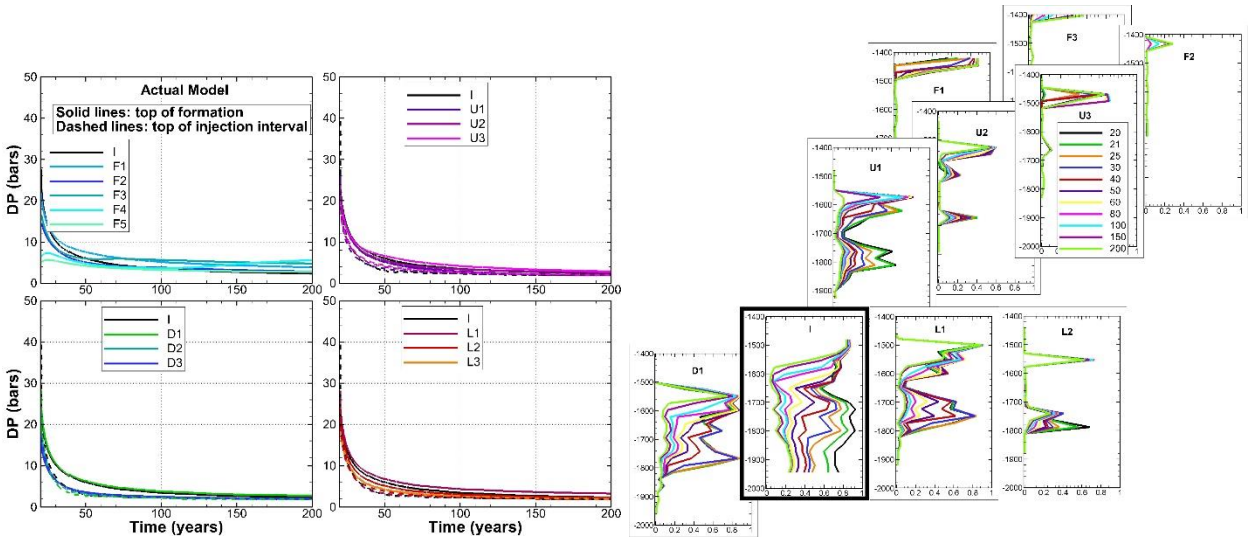

Figure 29. Actual model pressure transients (left) and saturation profiles (right) for the entire post-injection simulation period.

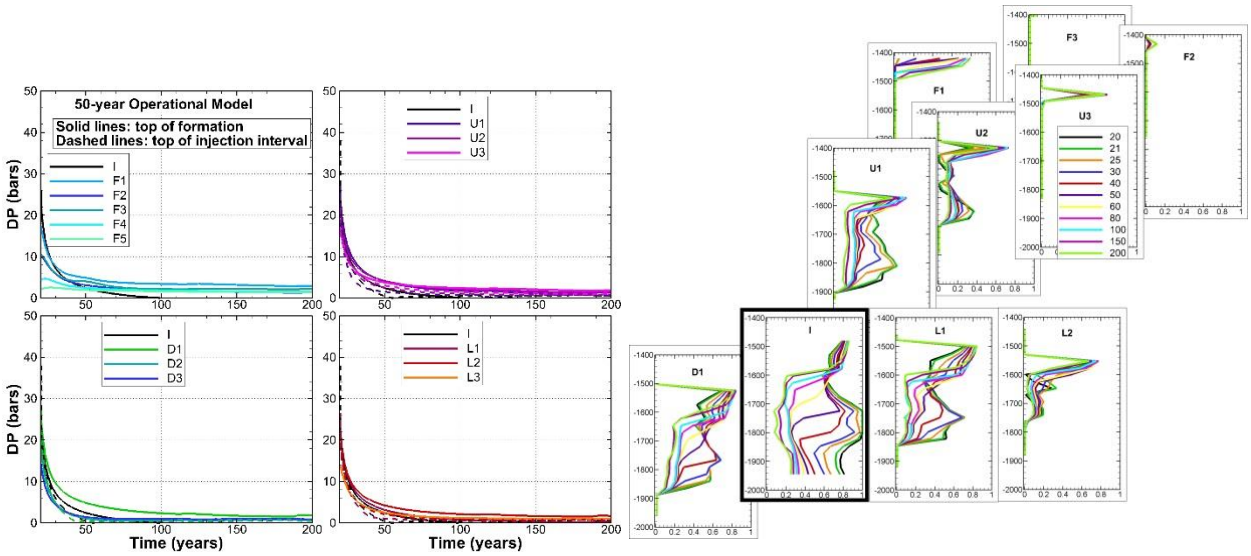

Figure 30. Fifty-year operational model pressure transients (left) and saturation profiles (right) for the entire post-injection simulation period.

549 Table 2. Summary of development of operational models.

Year	Change in Saturation Profile*	Operational Model at Start of Year's Development	Observations from Operational Model		Changes Made to Operational Model	Num-ber of Iter-ations
			Pressure transients	Saturation profiles		
1	**I**	Permeability 24 mD, no layering, no faults, no lateral heterogeneity, non-hysteretic relative permeability, no CH_4	*dP* too big near I, too small far from I	$S_g(z)$ too uniform at I	Increase permeability; introduce layering at perforated interval	6
2	I, **L1**, **D1**	Layering at perforated interval (3 - 121 mD), permeability 121 mD above perforated interval	*dP* at I perforated interval too big; *dP* at L3 too big	S_g peaks at L1 and D1 late arriving; S_g peak above perforated interval in I is missing	Modify permeability layering at perforated interval; introduce layering above perforated interval; Introduce fault between L2 and L3	3
3	I, L1, D1, **U1**	Layering at perforated interval (2 mD – 300 mD), layering above perforated interval (100 – 150 mD), L2/L3 fault permeability 5 mD	*dP* too big near I	S_g peaks okay, but too broad	Modify permeability layering; increase permeability at perforated interval, decrease permeability shallow	3
5	I, L1, D1, U1	Layering at perforated interval (4 mD – 600 mD), layering above perforated interval (50 – 150 mD), fault permeability 15 mD	Curvature of *P* vs *t* too large; *dP* at I perforated interval too small	S_g peaks okay, but too broad	Modify permeability layering: decrease permeability just above perforated interval; include CH_4	8

10	I, L1, **L2**, D1, U1, **U2**	Layering at perforated interval (4 mD – 600 mD), layering above perforated interval (25 – 141 mD), fault permeability 15 mD; CH_4 included	*dP* generally too small; curvature unchanged	S_g peaks at perforated interval okay, shallow CO_2 peaks too small	Modify permeability layering: decrease permeability at perforated interval and increase permeability shallow; Introduce fault west of well field; increase permeability of L2/L3 fault	6
20	I, L1, L2, D1, U1, U2, **F1**	Layering at perforated interval (3 mD – 400 mD), layering above perforated interval (50– 500 mD), L2/L3 fault permeability 30 mD; west fault permeability 1 mD; CH_4 included	Curvature a little smaller, but still too large; *dP* generally okay at 20 years	S_g profiles generally good for both CO_2 and CH_4	Extend both faults farther updip	1
25	I, L1, L2, D1, U1, U2, **U3**, F1	Same as 20 years except faults extended in updip direction. Non-hysteretic model with $S_{gr} = 0.2$ during post-injection period	Curvature a little smaller	S_g profiles do not decrease enough from their maximum during early post-injection period	Double rock compressibility; eliminate non-hysteretic model with $S_{gr} = 0.2$ during post-injection period; develop non-hysteretic model with $S_{gr} = 0$ during post-injection period and hysteretic model with $S_{grmax} = 0.2$	3

50	I, L1, L2, D1, U1, U2, U3, F1	Same as 25 years except rock compressibility doubled to 0.6e-8; non-hysteretic model with $S_{gr} = 0$, hysteretic model with $S_{grmax} = 0.2$	Curvature a little smaller; *dP* still too small at far wells; no significant effect of hysteresis	Non-hysteretic model with $S_{gr} = 0$: S_g profiles decrease too much near $S_g = 0.2$	Eliminate non-hysteretic model with $S_{gr} = 0$	2
100	I, L1, L2, D1, U1, U2, U3, F1, **F2**, **F3**	Same as 50 years, but hysteretic model only	*dP* all approach-ing zero	S_g changes getting smaller		1

*Bold indicates the first time a well shows a saturation change

4.3 Two Key Operational Model Metrics

After each operational model shown in Table 2 was completed, it was used to simulate the entire period from zero to 200 years. The two key metrics obtained from these simulations are the radius of the CO_2 plume (R_0, where S_g and CO_2 mass fraction are at least 0.02) as a function of time, and the radius at which the pressure response is big enough to drive fluid through a hypothetical flow path in the caprock (R_1, where $dP \geq 1$ bar), which occurs at the end of the injection period (20 years). These two key metrics also define Area of Review under the U.S. EPA Class VI well regulation (U.S. EPA, 2013).

Figure 31 plots the ratio of R_0 for the operational and actual models as a function of time for each operational model. A ratio less than one indicates that the operational-model plume does not migrate as far updip as the actual-model plume, and this is the result for all the early operational models. Later operational models under-predict plume migration at early times, but slightly over-predict it at later times. Two results are shown for the initial operational model (Year 0) and the twenty-five-year operational model, both of which are non-hysteretic, one with $S_{gr} = 0$ during the

post-injection period, and the other with S_{gr} = 0.2. The fifty-year operational model is a hysteretic model, with history-dependent S_{gr}, and as expected, its results are bracketed by the two twenty-five-year non-hysteretic models. The large difference between the ratios for the twenty-five-year non-hysteretic models (orange curves) is one indication that using a hysteretic model helps reduce uncertainty in plume-migration prediction. If one had used the difference between the initial non-hysteretic models (purple curves) to judge the importance of including hysteresis, the small difference would have been misleading because the updip migration of the initial plume is so small (less than 20% of the actual migration) that there is little opportunity for hysteretic effects to come into play.

Figure 32 plots the ratio of R_0 for the operational and actual models for 200 years, as a function of the year the model was developed, illustrating the gradual decrease in uncertainty in CO_2 updip migration as more data are used to improve the operational model. Early models severely underpredict the extent of the CO_2 plume, whereas later models overpredict it slightly. Although a good match would obviously the best outcome, overprediction of plume extent is preferable to underprediction in terms of being conservative. Figure 32 also shows the analogous plot for the pressure response R_1 for 20 years, again illustrating a gradually decreasing trend in uncertainty. Generally, the trend in R_1 is similar to that for R_0, showing that uncertainty in CO_2 plume migration and pressure response behave comparably: the initial operational model produces a poor prediction of actual model behavior, while using 1-3 years of monitoring data improves operational model predictions somewhat, using 5 years improves them more, and by 10 years the operational model is significantly closer to the actual model. Using data collected between 10 and 25 years further improves the operational model.

Figure 32 also illustrates how the monitoring-well pressure mismatch between operational and actual models is manifested as an error in the extent of the pressure pulse. For the final operational model, the pressure error at the end of the injection period (compare Figure 24 and Figure S24 in the supplemental material) is typically no more than one or two bars near the injection well, but increases to as much as 5 bars farther away, with the operational model underpredicting pressure response. Figure 32 shows that the extent of the pressure pulse for the final operational model is about 85% of the actual model radial extent. Given the importance of properly estimating the extent of the pressure pulse for Area of Review considerations, observations from more distant monitoring wells are essential. Further complicating the issue is that local variations in permeability produce local variations in pressure response, making it valuable to employ multiple pressure monitoring locations.

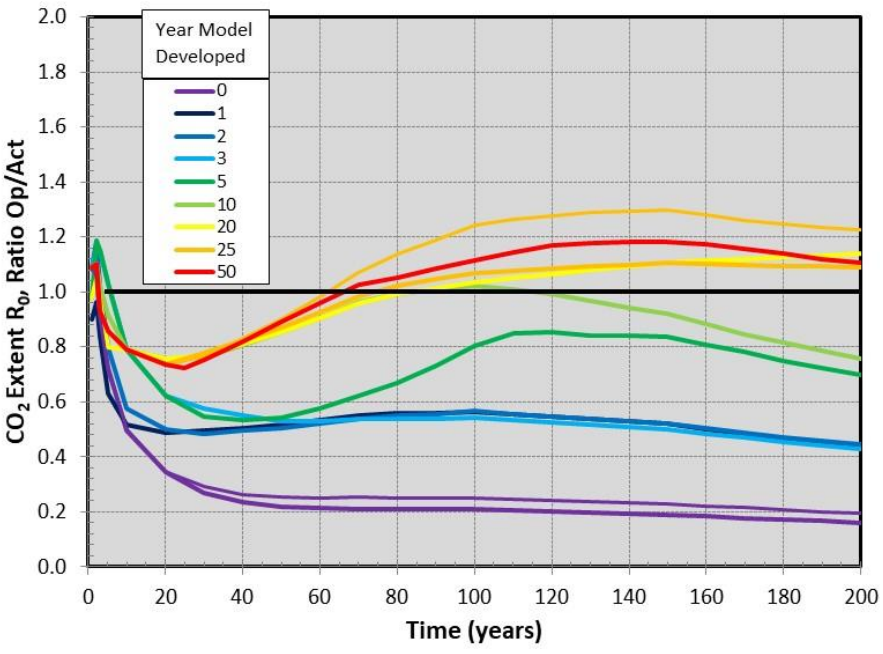

Figure 31. Ratio of the updip CO_2 plume migration R_0 for operational (Op) and actual (Act) models, as a function of time. Values less than one indicate the operational model does not move as far updip as the actual model. The legend identifies the year the operational model was developed. For the 0- and 25-year operational models, the thinner line has $S_{gr} = 0$ and the thicker line has $S_{gr} = 0.2$.

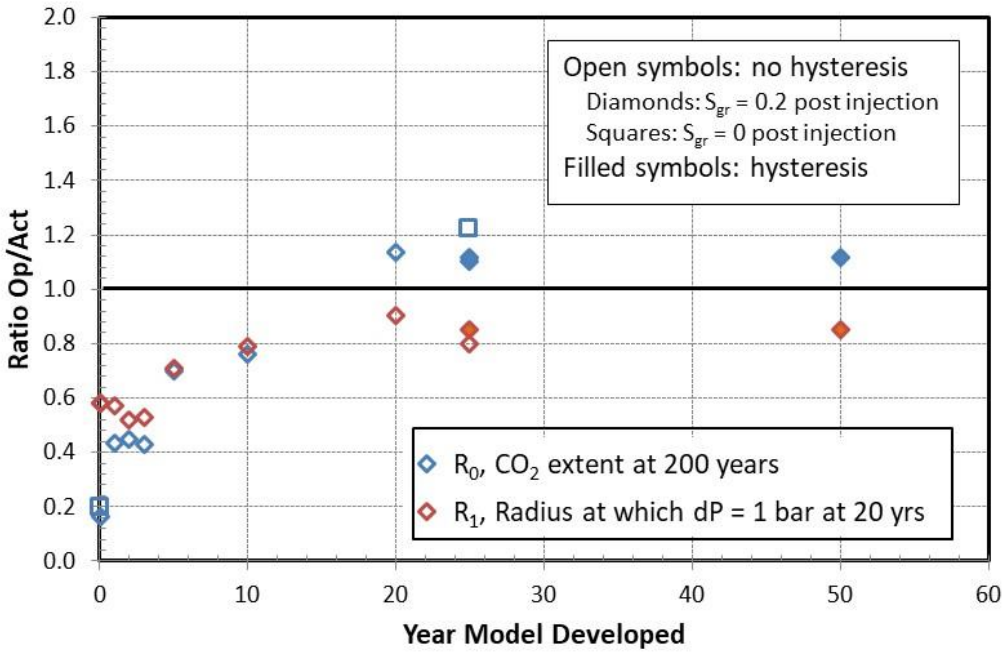

Figure 32. Ratios of R_0 and R_1 for operational (Op) and actual (Act) models, with the horizontal axis indicating the year the operational-model was developed. Values of R_0 less than one indicate the operational-model CO_2 plume does not move as far updip as in the actual model.

5. Discussion

The hypothesis investigated in this study is that uncertainties in forecasts of CO_2 plume evolution and pressure change decrease over time as more monitoring data are collected and incorporated into operational models. The key features of the pressure transients examined (and the model properties they inform) are:

- magnitude of overall pressure change (horizontal permeability)
- difference between responses at monitoring wells that are near the injection well and those that are farther away (horizontal permeability)
- difference between responses at the perforated interval and at the top of the formation (vertical permeability)
- curvature of the *dP* versus time plots (flow field geometry, storativity).

An important point to note about the saturation profiles is that the operational model profiles tend to show saturation peaks at the same depths, because the operational model is layered,

whereas the actual model shows saturation peaks at different depths, because the lateral and vertical heterogeneity enables irregular fluid flow paths upward and updip through the formation under buoyancy forces. Thus rather than comparing the exact depth of saturation peaks, we try to match the general trend of peaks developing first at the perforated interval near the injection well, and moving gradually upward and updip, which is sensitive to both horizontal and vertical permeability.

We present in Figures 33 and 34 a compact summary of the evolution of uncertainty of these key measures of GCS system changes. The plots show concordance at selected monitoring locations at three different times through the plotting of pressure change and gas saturation for the series of operational models developed over time (different colored circles) normalized by the actual-model values at those same locations and times. For pressure change, monitoring times during the CO_2 injection period are most relevant, whereas for gas saturation, later monitoring times (e.g., post-injection times when the CO_2 plume has reached many monitoring wells) are of more interest. For example, in Figure 33 the purple circles labeled with a zero represent the initial model (model developed at year zero) and the corresponding normalized results from that initial model are shown at selected times during the CO_2 injection period: 1 year, 5 years, and 20 years. Similarly, the dark blue, medium blue, light blue circles represent the years 1, 2, 3, respectively, that the model was updated. Figure 33 shows that despite some scatter, operational model colors (year of development) show a general trend of migration of the forecasted pressure differences toward the line where operational normalized by actual equals unity. Figure 34 shows analogous results for saturation in the top layer at three different times after injection ceases. The trend toward better concordance (reduced uncertainty) with color is not as clear for the saturation as for pressure because saturation is much more sensitive to local permeability heterogeneity in the

644 model. Nevertheless, there is improvement over model-development time at many locations, and
645 this result mimics what would actually be observed in field data that are limited and subject to
646 vagaries of measurement location in a heterogeneous natural system. Overall, Figures 33 and 34
647 make the point that uncertainty in the plume's future migration and effects on the subsurface are
648 large at the beginning, but with competent monitoring and updating of operational models, the
649 uncertainty trends downward over time.

650 Some details of the particular system we studied may be generally useful for cases of GCS in
651 depleted natural gas reservoirs. For example, we observed that when both CH_4 and CO_2 are
652 included in the model, distant monitoring wells show a distinctive signal of a CH_4 arrival
653 presaging the CO_2 arrival. This effect has been observed and modeled previously (e.g.,
654 Oldenburg et al., 2013). We also found that the decline of saturation peaks in the post-injection
655 period requires imbibition and capillary trapping to be properly modeled.

656 Table 2 shows the year when the CO_2 plume reaches each monitoring well, indicating that for the
657 first three years, CO_2 reaches only the nearest three wells (D1, L1, and U1). The CO_2 plume
658 reaches only five wells during the first 10 years of injection, and only six wells by the end of the
659 injection period at 20 years. This sequence suggests the idea of initially drilling only a few
660 monitoring wells near the injection well, then adding more monitoring wells as the CO_2 plume
661 grows. Adding one or two new monitoring wells every 5-10 years, with locations informed by
662 previous plume development, should be a cost-effective approach to monitoring CO_2 plume
663 migration. In contrast, the pressure-transient information provided by distant wells is useful
664 even at early times. Thus, a good initial monitoring well configuration might consist of three
665 nearby wells (e.g., D1, L1, U1), and one or two more distant well (e.g., F3, F4). Another
666 possibility for minimizing the number of monitoring wells would be to augment monitoring-well

observations with time-lapse geophysical surveys (e.g., Doughty and MacLennan, 2018; Pevzner et al., 2011; Daley et al., 2011).

Perfect concordance between operational and actual model pressure transients and saturation profiles is not expected given the significant lateral heterogeneity of the actual model (e.g., Figures 2 and S2) which is not included in the operational models. Of course, pressure-transient data from multiple wells can be inverted to estimate heterogeneous permeability distributions, but with pressure data from only two depths (the top of the perforated interval and the top of the storage formation), and local permeability values required for more than 20 model layers, this would be an ill-posed inverse problem, requiring sophisticated inverse methods. Doing a joint inversion of pressure-transient and saturation profile data is also a possibility, but again would require advanced inverse methods. Such approaches are not in keeping with our conceptual model of field operators using and updating (improving) relatively simple numerical models. Instead, we acknowledge that concordance will not be perfect, and try to improve the model by looking at general trends in the pressure transients and saturation profiles, as described in the previous section, just as operators are expected to do.

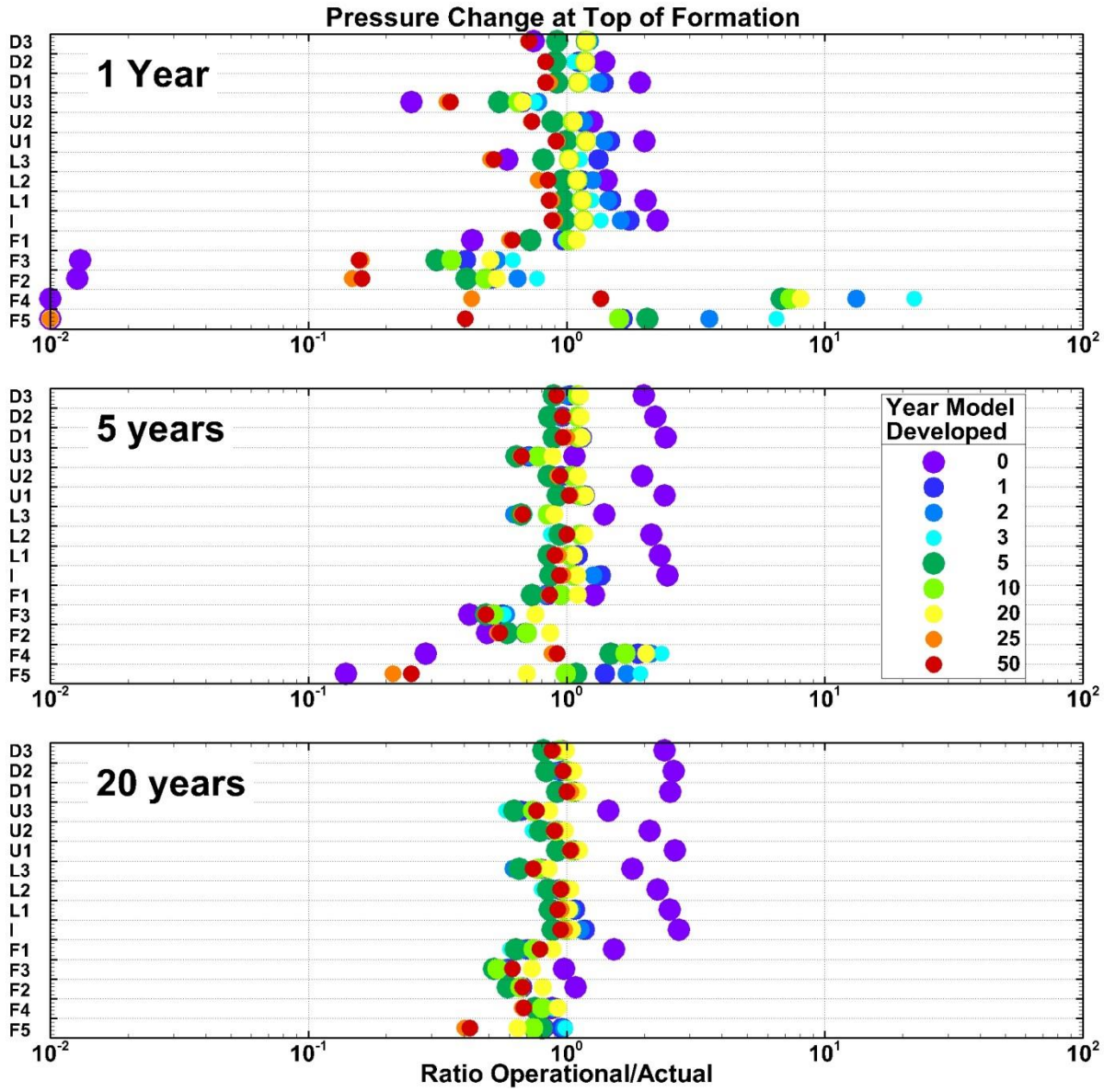

Figure 33. Ratio of pressure change (operational/actual) at three times for each monitoring well for the sequence of operational models (color identifies the year the model was developed), showing general evolution toward the line where operational/actual equals one. Symbols are slightly different sizes for better visibility of tightly grouped symbols.

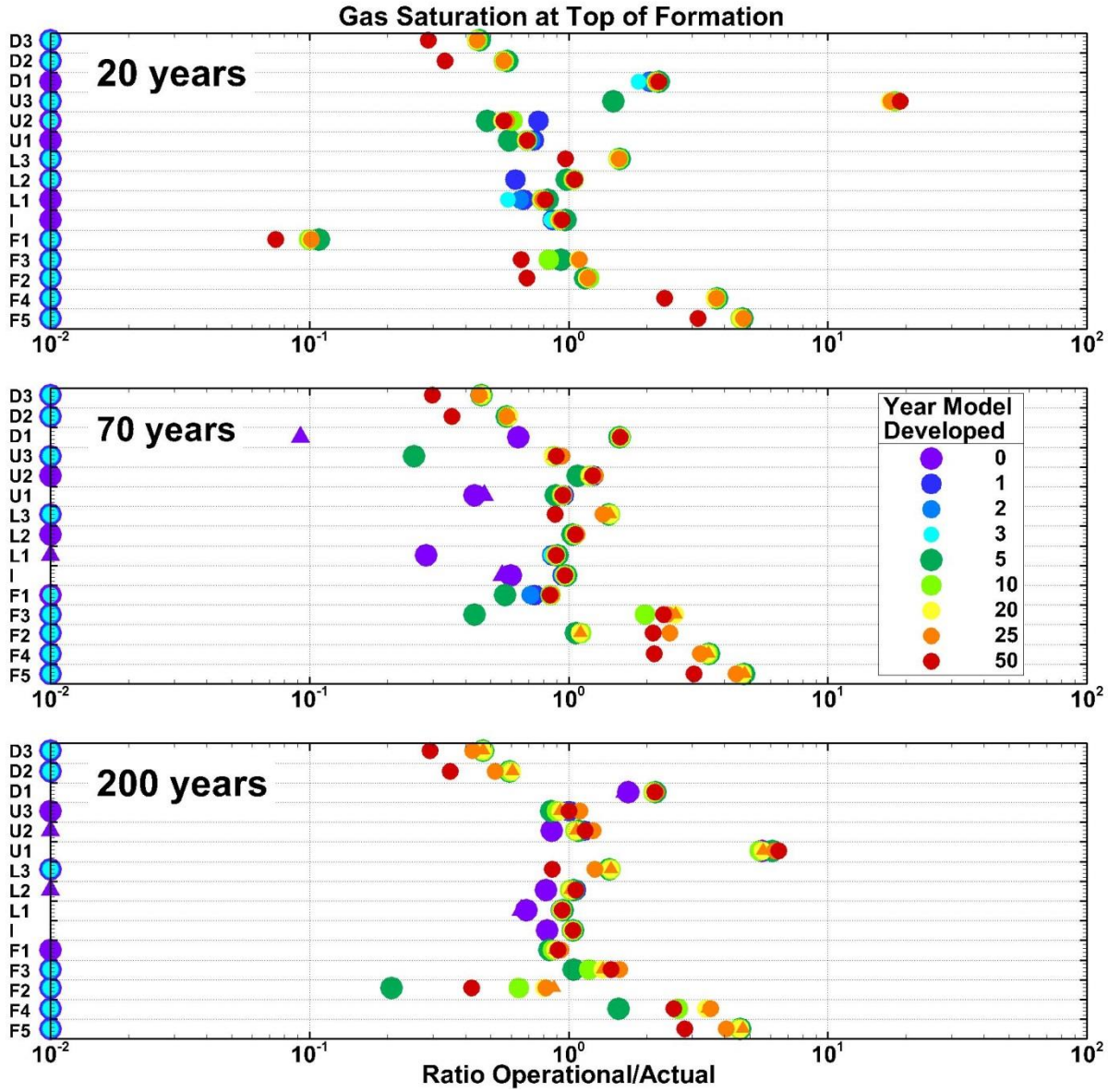

Figure 34. Ratio of saturation at top of storage formation (operational/actual) at three times for each monitoring well, for the sequence of operational models (color identifies the year the model was developed), showing general evolution toward the line where operational/actual equals one. For the non-hysteretic models, two values of residual gas saturation are shown: circles indicate $S_{gr} = 0$ and deltas indicate $S_{gr} = 0.2$. Symbols are slightly different sizes for better visibility of tightly grouped symbols.

6. Conclusions

We have illustrated the year-by-year improvement to an initially simple operational model of CO_2 sequestration in a depleted natural gas reservoir. The analysis of each year's pressure-transient and saturation-profile data and comparison to synthetic data created using a more complex model, denoted the actual model, provides the impetus for modifications to the operational model. Two key metrics represent the ability of the operational model to accurately predict the results of the actual model: the extent of the CO_2 plume up-dip migration, and the radial extent of the pressure pulse. Deviations between the actual and operational models for both of these metrics steadily decrease as more monitoring data become available over time. While the goal of this paper was to show the reduction in uncertainty that occurs when models are updated and improved based on operational data, the process by which we demonstrated this reduction in uncertainty also illustrates a workflow that may set a useful example for site operators.

The summary plots (Figures 31 – 34) indicate that for a twenty-year injection period, using monitoring data for the first 10 years greatly improves the ability of the operational model to predict the 50-year PISC period and out to the end of the entire 200 year simulation. In fact, data from the first year are already valuable, especially in constraining near-injection-well properties. However, including data from the post-injection period is mandatory for understanding both the drainage and imbibition aspects of CO_2 plume migration. For the present example with a high-permeability storage formation and significant up-dip CO_2 migration, it was necessary to use a hysteretic model to properly account for both of these processes. Some of the parameters of the hysteretic model could be inferred from just the first five years of the post-injection period when

the saturation peaks first began to decrease, but a clearer picture emerged by considering longer post-injection times around 50 years, when saturation values neared the residual saturation.

Acknowledgements and Disclaimer

We thank Jeff Wagoner of Lawrence Livermore National Laboratory for providing the geologic model of the Southern Sacramento River Delta region, Diana Bacon (PNNL) and Christopher Brown (PNNL) for constructive reviews of an earlier draft, and two anonymous reviewers. This work was supported by the Assistant Secretary for Fossil Energy, Office of Sequestration, Hydrogen, and Clean Coal Fuels, for the National Risk Assessment Partnership (NRAP) project managed by the National Energy Technology Laboratory (NETL). Additional support came from the U.S. Department of Energy under Contract No. DE-AC02-05CH11231. This report was prepared as an account of work sponsored by an agency of the United States Government.

References

Burton, E., Mateer, N., Myhre, R., and Stone, M., 2016. WESTCARB Phase III final report, summary of California activities, California Energy Commission Report CEC-500-2016-053, 49 pp.

California Air Resources Board, 2017. Carbon capture and sequestration protocol under the Low Carbon Fuel Standard. https://www.arb.ca.gov/fuels/lcfs/ccs_protocol_010919.pdf

Chadwick, R.A. and Noy, D.J., 2015. Underground CO_2 storage: demonstrating regulatory conformance by convergence of history-matched modeled and observed CO_2 plume behavior using Sleipner time-lapse seismics. *Greenhouse Gases: Science and Technology*, *5*(3), pp.305-322.

Chen, Y. and Zhang, D., 2006. Data assimilation for transient flow in geologic formations via ensemble Kalman filter. *Advances in Water Resources*, *29*(8), pp.1107-1122.

Daley, T.M., Ajo-Franklin, J.B. and Doughty, C., 2011. Constraining the reservoir model of an injected CO_2 plume with crosswell CASSM at the Frio-II brine pilot. *International Journal of Greenhouse Gas Control*, 5(4), pp.1022-1030.

Deutsch, C.V. and Journel, A.G., 1992. *Geostatistical Software Library and User's* Guide (2nd Ed.). Oxford University Press, New York.

Doughty, C., 2007. Modeling geologic storage of carbon dioxide: comparison of hysteretic and non-hysteretic curves, *Energy Conversion and Management*, *48*(6), pp.1768-1781.

Doughty, C. and MacLennan, K., 2018. Using TOGA to model CO_2-EOR in conjunction with time-lapse electromagnetic monitoring, TOUGH Symposium 2018, Lawrence Berkeley National Lab., Berkeley CA, October 8-10.

Doughty, C. and Oldenburg, C.M., 2019. Carbon dioxide plume evolution following injection into a depleted natural gas reservoir: modeling of conformance uncertainty reduction over time, *Rep. LBNL-2001228*, Lawrence Berkeley National Laboratory, Berkeley, CA.

Foxall, W., Doughty, C., Lee, K.J., Nakagawa, S., Daley, T., Burton, E., Layland-Bachmann, C., Borglin, S., Freeman, K., Ajo-Franklin, J., Jordan, P., Kneafsey, T., Oldenburg, C., Ulrich, C., 2017. Investigation of potential induced seismicity related to geologic carbon dioxide sequestration in California, California Energy Commission Report CEC-500-2017-028.

Freifeld, B.M., Trautz, R.C., Kharaka, Y.K., Phelps, T.J., Myer, L.R., Hovorka, S.D. and Collins, D.J., 2005. The U-tube: A novel system for acquiring borehole fluid samples from a deep geologic CO_2 sequestration experiment. *Journal of Geophysical Research: Solid Earth*, *110*(B10).

Harp, D.R., Oldenburg, C.M. and Pawar, R., 2019. A metric for evaluating conformance robustness during geologic CO_2 sequestration operations. *International Journal of Greenhouse Gas Control*, 85, pp.100-108.

IPPC, 2018. Global warming of 1.5°C. An IPCC Special Report on the impacts of global warming of 1.5°C above pre-industrial levels and related global greenhouse gas emission pathways, in the context of strengthening the global response to the threat of climate change, sustainable development, and efforts to eradicate poverty [Masson-Delmotte, V., P. Zhai, H.-O. Pörtner, D. Roberts, J. Skea, P.R. Shukla, A. Pirani, W. Moufouma-Okia, C. Péan, R. Pidcock, S. Connors, J.B.R. Matthews, Y. Chen, X. Zhou, M.I. Gomis, E. Lonnoy, T. Maycock, M. Tignor, and T. Waterfield (eds.)].

Jung, Y., Pau, G.S.H., Finsterle, S. and Pollyea, R.M., 2017. TOUGH3: A new efficient version of the TOUGH suite of multiphase flow and transport simulators. *Computers & Geosciences*, 108, pp.2-7.

Keating, E.H., Doherty, J., Vrugt, J.A. and Kang, Q., 2010. Optimization and uncertainty assessment of strongly nonlinear groundwater models with high parameter dimensionality. *Water Resources Research*, *46*(10), W10517.

Oladyshkin, S., Class, H., Helmig, R. and Nowak, W., 2011. A concept for data-driven uncertainty quantification and its application to carbon dioxide storage in geological formations. *Advances in Water Resources*, *34*(11), pp.1508-1518.

Oldenburg, C.M., 2018. Are we all in concordance with the meaning of the word conformance, and is our definition in conformity with standard definitions? *Greenhouse Gases: Science and Technology*, *8*(2), pp.210-214.

Oldenburg, C.M., Doughty, C. and Spycher, N., 2013. The role of CO_2 in CH_4 exsolution from deep brine: Implications for geologic carbon sequestration. *Greenhouse Gases: Science and Technology*, 3(5), pp.359-377.

Oldenburg, C.M., Moridis, G.J., Spycher, N. and Pruess, K., 2004. EOS7C Version 1.0: TOUGH2 module for carbon dioxide or nitrogen in natural gas (methane) reservoirs, *Rep. LBNL-56589*, Lawrence Berkeley National Laboratory, Berkeley, CA .

Oldenburg, C.M., Pruess, K. and Benson, S.M., 2001. Process modeling of CO_2 injection into natural gas reservoirs for carbon sequestration and enhanced gas recovery. *Energy & Fuels*, *15*(2), pp.293-298.

Pevzner, R., Shulakova, V., Kepic, A. and Urosevic, M., 2011. Repeatability analysis of land time-lapse seismic data: CO2CRC Otway pilot project case study. *Geophysical Prospecting*, 59(1), pp.66-77.

Sun, A.Y., Morris, A.P. and Mohanty, S., 2009. Sequential updating of multimodal hydrogeologic parameter fields using localization and clustering techniques. *Water Resources Research*, *45*(7), W07424.

U.S. EPA (United States Environmental Protection Agency), 2008. Federal requirements under the underground injection control (UIC) program for carbon dioxide (CO_2) geologic sequestration (GS) Wells, Proposed Rule, 40 CFR Parts 144 and 146, EPA-HQ-OW-2008-0390.

U.S. EPA, 2013. Geologic sequestration of carbon dioxide underground injection control (UIC) program Class VI well area of review evaluation and corrective action guidance, Office of Water (4606M), EPA 816-R-13-005.

van Genuchten, M.Th., 1980. A closed-form equation for predicting the hydraulic conductivity of unsaturated soils. *Soil Science Society of America Journal*, *44*(5), pp. 892-898.

Walter, L., Binning, P.J., Oladyshkin, S., Flemisch, B. and Class, H., 2012. Brine migration resulting from CO_2 injection into saline aquifers–An approach to risk estimation including various levels of uncertainty. *International Journal of Greenhouse Gas Control*, *9*, pp.495-506.